J. Fluid Mech. (2008), *vol.* 596, *pp.* 73–101.
doi:10.1017/S002211200700924X Printed in the United Kingdom

Optimal growth and transition to turbulence in channel flow with spanwise magnetic field

DMITRY KRASNOV[1], MAURICE ROSSI[2], OLEG ZIKANOV[3] AND THOMAS BOECK[1]

[1]Fakultät Maschinenbau, Technische Universität Ilmenau, Postfach 100565, 98684 Ilmenau, Germany

[2]Institut Jean Le Rond D'Alembert, Université Pierre et Marie Curie, 4 place Jussieu, F-75252 Paris Cedex 05, France

[3]Department of Mechanical Engineering, University of Michigan - Dearborn, 4901 Evergreen Road, Dearborn, MI 48128-1491, USA

(Received 11 December 2006 and in revised form 30 August 2007)

Instability and transition to turbulence in a magnetohydrodynamic channel flow are studied numerically for the case of a uniform magnetic field imposed along the spanwise direction. Optimal perturbations and their maximum amplifications over finite time intervals are computed in the framework of the linear problem using an iterative scheme based on direct and adjoint governing equations. It is shown that, at sufficiently strong magnetic field, the maximum amplification is no longer provided by classical streamwise rolls, but rather by rolls oriented at an oblique angle to the basic flow direction. The angle grows with the Hartmann number Ha and reaches the limit corresponding to purely spanwise rolls at Ha between 50 and 100 depending on the Reynolds number. Direct numerical simulations are applied to investigate the transition to turbulence at a single subcritical Reynolds number $Re = 5000$ and various Hartmann numbers. The transition is caused by the transient growth and subsequent breakdown of optimal perturbations, which take the form of one or two symmetric optimal modes (streamwise, oblique or spanwise modes depending on Ha) with low-amplitude three-dimensional noise added at the moment of strongest energy amplification. A sufficiently strong magnetic field (Ha larger than approximately 30) is found to completely suppress the instability. At smaller Hartmann numbers, the transition is observed but it is modified in comparison with the pure hydrodynamic case.

1. Introduction

In this paper we consider the transition to turbulence in a pressure-driven flow of an electrically conducting fluid within a plane channel. The flow is affected by a steady uniform magnetic field imposed in the spanwise (parallel to the wall and perpendicular to the flow) direction. This flow can be viewed as an idealized model of flows in the presence of a magnetic field with non-zero component parallel to solid walls. Such flows can be found in numerous metallurgical and materials processing applications. Prominent examples include the electromagnetic flow control in continuous steel casting (Davidson 1999; Thomas & Zhang 2001) and in the growth of large silicon crystals (von Ammon *et al.* 2005). Another area of applications is the liquid-metal (Li or Pb-17Li) cooling blankets of breeder type for fusion reactors (Barleon *et al.* 2001). Typical blanket design includes a duct flow in a strong imposed magnetic field.

Instability and transition to turbulence in sidewall boundary layers (with respect to which the magnetic field is spanwise) is one of the possible ways to achieve the desired intensification of heat and mass transfer. From a different application viewpoint, Lee & Choi (2001) have shown that a spanwise magnetic field can lead to substantial reduction of the turbulent drag in a channel flow.

We assume that the magnetic Reynolds number $Re_m \equiv U L \sigma \mu$ is small, where U and L are the typical velocity and length scales, σ is the electric conductivity of the fluid, and μ is the magnetic permittivity of vacuum. The assumption $Re_m \ll 1$ is valid for practically all industrial and laboratory flows of liquid metals and other electrically conducting fluids including those mentioned above. It allows us to simplify the problem significantly by justifying the use of the quasi-static approximation (Roberts 1967). The fluctuations of the magnetic field due to the fluid motion are much weaker than the imposed magnetic field and can be assumed to adjust instantaneously to the velocity fluctuations.

The general effect of the imposed magnetic field on a low-Re_m flow can be identified as two-fold (see, e.g., Moreau 1990; Davidson 2001). First is the flow suppression by Joule dissipation of induced electric currents. The second effect is the introduction of anisotropy due to the suppression acting preferentially on the flow modes with strong gradients in the direction of the magnetic field. No electric currents are generated and no Joule dissipation occurs in a two-dimensional flow uniform along the magnetic field lines.

The anisotropic character of the Joule dissipation makes the case of a channel in a spanwise field particularly interesting for the general theory of instability and transition. While leaving the basic velocity profile unchanged, the magnetic field can transform the evolution of stable or unstable perturbations and, more generally, the properties of the transition. The applied magnetic field renders the spanwise direction preferable in the sense that perturbations which are uniform in this direction are not directly affected, in particular, not suppressed by the magnetic field. This results in a different symmetry of the problem and, as demonstrated in our paper, in a modification of the transition.

Among the possible transition scenarios, we focus on the one based on the algebraic transient growth of optimal perturbations and their subsequent three-dimensional breakdown. The scenario was shown to be pertinent in parallel shear flows, such as boundary layers (Schmid & Henningson 2001), plane Poiseuille flow (Reddy *et al.* 1998) or pipe Poiseuille flow (Zikanov 1996). The underlying concept is that of transient algebraic growth experienced by certain solutions of the linear perturbation problem even far below the linear stability threshold. In the flows mentioned above, the optimal perturbations have the form of two-dimensional streamwise rolls that evolve into streamwise streaks via the lift-up mechanism. The amplification of the strongest growing (optimal) perturbations can be sufficiently large that, considered in the framework of the full nonlinear problem, the perturbations may result in the modification of the basic flow rendering it temporarily unstable, either exponentially or in a transient algebraic way, to three-dimensional perturbations. This secondary instability, also referred to as streak breakdown, leads to turbulence.

The effect of an applied magnetic field on the transient growth and the breakdown scenario has been analysed for the case of Hartmann flow (channel flow of an electrically conducting fluid in the presence of a uniform magnetic field). Gerard-Varet (2002) considered the purely streamwise optimal perturbations in the framework of the linear model and the quasi-static approximation. The work was continued by Airiau & Castets (2004), where the full magnetohydrodynamic (MHD) equations were

solved and the effect of the magnetic Reynolds number was investigated. In addition, Krasnov *et al.* (2004) conducted nonlinear simulations of the streak breakdown and the subsequent transition. It should be stressed that the configuration considered in the present paper differs from that of the Hartmann flow in a fundamental way. In a Hartmann channel, the magnetic field affects the basic flow and the linear stability. The transition based on the transient growth and three-dimensional breakdown is affected by the magnetic field, but remains the same as in the non-magnetic case in its principal aspects. In particular, the optimal modes retain their shape of streamwise rolls evolving into streamwise streaks. In our case, the spanwise magnetic field does not affect the basic flow or its linear instability to Tollmien–Schlichting waves. It does, however, modify the transition caused by the transient growth. As will be shown in the paper, the key feature of the modification is the preferential suppression of streamwise modes, which allows oblique or even spanwise modes to become dominant modes of the transition.

After formulating the problem in § 2, we analyse the transient evolution of linear perturbations in §§ 3 and 4. We use the adjoint procedure to determine the optimal perturbations. It should be stressed that, owing to the effect of the spanwise magnetic field, arbitrary three-dimensional perturbations should be considered. In § 5, the nonlinear evolution of such optimal modes and transition to turbulence triggered by superposition of one or two families of the symmetric optimal modes and three-dimensional noise are investigated through direct numerical simulations (DNS).

2. Governing equations

Let us consider the flow of an incompressible electrically conducting fluid in an infinite plane channel between insulating walls located at $z = \pm d/2$, where x, y and z denote the streamwise, spanwise and cross-stream directions, respectively. The flow is driven by a pressure gradient $\partial P_0/\partial x$ in the x-direction and subjected to a constant spanwise magnetic field $\boldsymbol{B}_0 = B_0\boldsymbol{e}$, where $\boldsymbol{e} \equiv (0, 1, 0)$.

With the assumption of low magnetic Reynolds number, the governing equations reduce to the Navier–Stokes system for the velocity $\boldsymbol{v}$ and pressure p with the additional Lorentz force $\boldsymbol{j} \times \boldsymbol{B}_0$, where the induced electric current density is given by the Ohm law

$$\boldsymbol{j} = \sigma(-\nabla\phi + \boldsymbol{v} \times \boldsymbol{B}_0). \tag{2.1}$$

Neglecting displacement currents and assuming that the fluid is electrically neutral we require that $\nabla \cdot \boldsymbol{j} = 0$. This leads to an equation for the electric potential ϕ:

$$\nabla^2\phi = \nabla \cdot (\boldsymbol{v} \times \boldsymbol{B}_0). \tag{2.2}$$

The problem is solved in a rectangular domain with periodicity conditions used in the x- and y-directions following the assumption of flow homogeneity. The no-slip conditions are imposed at the walls. The electric potential ϕ is also periodic in the x- and y-directions. Since no current flows through the electrically insulating walls and the velocity $\boldsymbol{v}$ is zero at these walls, (2.1) leads to

$$\frac{\partial\phi}{\partial z} = 0 \quad \text{at } z = \pm d/2. \tag{2.3}$$

It is important to stress that a uniform spanwise magnetic field does not affect the basic Poiseuille flow or any other flow with velocity field independent of the spanwise coordinate. This can be easily verified by taking curl of Ohm's law (2.1), which leads

to

$$\nabla \times \boldsymbol{j} = \sigma(\boldsymbol{B}_0 \cdot \nabla)\boldsymbol{v} = 0.$$

The only solution in the absence of externally imposed currents is $\boldsymbol{j} = 0$. A spanwise-uniform flow does not induce any currents and evolves in a purely hydrodynamic manner.

The basic velocity field, thus, has the classical parabolic profile

$$U_H(z) = U\left(1 - \frac{4z^2}{d^2}\right), \quad U \equiv -\frac{d^2}{8\nu\rho}\frac{\partial P_0}{\partial x}, \tag{2.4}$$

with the basic pressure field $P_H(x) = (\partial P_0/\partial x)x$, the kinematic viscosity ν and the density ρ. Finally, the basic potential field is

$$\phi_H(z) = -\frac{d^2 B_0}{8\nu\rho}\frac{\partial P_0}{\partial x}\left(z - \frac{4z^3}{3d^2}\right). \tag{2.5}$$

For the non-dimensionalization, the centreline velocity U of the Poiseuille flow is used as the velocity scale. The characteristic length is taken to be the channel half-width $L \equiv d/2$. The imposed magnetic field and the electric potential scale with B_0 and LUB_0, respectively. Finally the units of time and pressure are taken as L/U and ρU^2. The non-dimensional basic velocity profile is $U_H(z) = 1 - z^2$, and the non-dimensional governing equations and boundary conditions become

$$\frac{\partial \boldsymbol{v}}{\partial t} - \boldsymbol{v} \times (\nabla \times \boldsymbol{v}) = -\nabla\left(p + v^2/2\right) + \frac{1}{Re}\nabla^2 \boldsymbol{v} + N\left(-\nabla\phi \times \boldsymbol{e} + (\boldsymbol{v} \times \boldsymbol{e}) \times \boldsymbol{e}\right), \tag{2.6}$$

$$\nabla \cdot \boldsymbol{v} = 0, \tag{2.7}$$

$$\nabla^2 \phi = \nabla \cdot (\boldsymbol{v} \times \boldsymbol{e}), \tag{2.8}$$

$$v_x = v_y = v_z = \frac{\partial \phi}{\partial z} = 0 \quad \text{at } z = \pm 1. \tag{2.9}$$

Two non-dimensional independent parameters can be defined, namely the Reynolds number

$$Re = \frac{UL}{\nu} = -\frac{d^3}{16\nu^2\rho}\frac{\partial P_0}{\partial x}, \tag{2.10}$$

and either the Hartmann number

$$Ha = \frac{d}{2\delta}, \quad \text{where } \delta = \frac{1}{B_0}\sqrt{\frac{\rho\nu}{\sigma}}, \tag{2.11}$$

or the magnetic interaction parameter

$$N \equiv \frac{Ha^2}{Re}. \tag{2.12}$$

Finally, integral conditions should be specified for the nonlinear evolution of perturbations and transition to turbulence. We assume that the volume flux Q_x per span width is constant.

3. Linear evolution of optimal perturbations

Let us now split the flow fields into a basic flow and three-dimensional perturbations as

$$\boldsymbol{v} = U_H(z)(1, 0, 0) + \boldsymbol{v}_p, \quad \phi = \phi_H(z) + \phi_p(x, y, z), \quad p = P_H(z) + p_p. \tag{3.1}$$

We linearize the system with respect to the perturbations and consider the evolution of decoupled monochromatic Fourier modes

$$(\boldsymbol{v}_p, \phi_p, p_p) = (\hat{u}(z,t), \hat{v}(z,t), \hat{w}(z,t), \hat{\phi}(z,t), \hat{p}(z,t)) \exp(\mathrm{i}\alpha x + \mathrm{i}\beta y), \tag{3.2}$$

where α and β are the wavenumbers in the streamwise (x) and spanwise (y) directions.

The evolution of such infinitesimal three-dimensional perturbations is governed by the linear system

$$\left[\frac{\partial}{\partial t} + \mathrm{i}\alpha U_H(z)\right]\hat{u} + \frac{\partial U_H}{\partial z}\hat{w} + \mathrm{i}\alpha\hat{p} - \frac{1}{Re}\left[\frac{\partial^2}{\partial z^2} - \alpha^2 - \beta^2\right]\hat{u} + N\hat{u} - N\frac{\partial\hat{\phi}}{\partial z} = 0, \tag{3.3}$$

$$\left[\frac{\partial}{\partial t} + \mathrm{i}\alpha U_H(z)\right]\hat{v} + \mathrm{i}\beta\hat{p} - \frac{1}{Re}\left[\frac{\partial^2}{\partial z^2} - \alpha^2 - \beta^2\right]\hat{v} = 0, \tag{3.4}$$

$$\left[\frac{\partial}{\partial t} + \mathrm{i}\alpha U_H(z)\right]\hat{w} + \frac{\partial\hat{p}}{\partial z} - \frac{1}{Re}\left[\frac{\partial^2}{\partial z^2} - \alpha^2 - \beta^2\right]\hat{w} + N\hat{w} + \mathrm{i}\alpha N\hat{\phi} = 0, \tag{3.5}$$

$$\mathrm{i}\alpha\hat{u} + \mathrm{i}\beta\hat{v} + \frac{\partial\hat{w}}{\partial z} = 0, \tag{3.6}$$

$$\left[\frac{\partial^2}{\partial z^2} - \alpha^2 - \beta^2\right]\hat{\phi} + \mathrm{i}\alpha\hat{w} - \frac{\partial\hat{u}}{\partial z} = 0 \tag{3.7}$$

with the boundary conditions

$$\hat{u} = \hat{v} = \hat{w} = 0, \quad \frac{\partial\hat{\phi}}{\partial z} = 0 \quad \text{at } z = \pm 1. \tag{3.8}$$

In this paper, we consider cases in which the flow is linearly stable, i.e. all eigensolutions of (3.3)–(3.8) decay exponentially. It is known from previous studies (see, e.g., Butler & Farrell 1992; Reddy *et al.* 1998) that, owing to the non-normality of the linear operator, the eigenmodes may form combinations that experience substantial transient algebraic growth before eventual decay. We focus on such perturbations and consider their amplification with the idea, further analysed in § 5, that transition to turbulence can be triggered by their nonlinear evolution. To quantify the amplification at time T, it is customary to define a norm, which is typically the kinetic energy of the perturbations. This norm can be orthogonally decomposed on a Fourier basis in the x- and y-directions, which implies that the individual contributions of each wavenumber pair (α, β) can be considered independently. We follow such a procedure and define the norm

$$E(T) \equiv \int (\hat{u}(z,T)\hat{u}^+(z,T) + \hat{v}(z,T)\hat{v}^+(z,T) + \hat{w}(z,T)\hat{w}^+(z,T))\,\mathrm{d}z \tag{3.9}$$

where the superscript + denotes complex conjugation, spatial integration is performed over the entire channel width, and the perturbations are obtained by time integration of the above linear system over the time period $[0, T]$.

The amplification gain of any given mode at time T is the ratio $E(T)/E(0)$. This quantity can be maximized over all possible initial vertical shapes in (3.2) to give the maximum amplification $\hat{G}(\alpha, \beta, T, Ha, Re)$ at time T among the disturbances with specific wavenumbers (α, β) and non-dimensional parameters Ha and Re. The search for the disturbance providing the maximum amplification, the so-called optimal disturbance, is the focus of the first part of our study. This problem can be solved using a standard technique of modal stability analysis. There is, however, a more convenient and efficient method (Farrell & Ioannou 1996; Andersson, Berggren & Henningson

1999; Luchini 2000; Schmid & Henningson 2001) that computes the maximum energy gain through an optimization procedure. One determines the optimum of $E(T)/E(0)$ with two constraints: (i) the disturbance energy $E(0)$ at time $t=0$ is equal to unity; (ii) the disturbance satisfies the linear governing equation as well as the boundary conditions during the complete time interval $[0, T]$. The solution can be obtained with the help of a Lagrangian formalism in which Lagrangian multipliers are introduced to enforce these constraints. In the present case, these multipliers are the adjoint fields $(\tilde{u}(z,t), \tilde{v}(z,t), \tilde{w}(z,t), \tilde{\phi}(z,t), \tilde{p}(z,t))$. Following a standard derivation† of the method, these quantities satisfy the adjoint equations:

$$\left[\frac{\partial}{\partial\tau} - \mathrm{i}\alpha U_H(z)\right]\tilde{u} - \frac{1}{Re}\left[\frac{\partial^2}{\partial z^2} - \alpha^2 - \beta^2\right]\tilde{u} + N\tilde{u} - \mathrm{i}\alpha\tilde{p} + \frac{\partial\tilde{\phi}}{\partial z} = 0, \tag{3.10}$$

$$\left[\frac{\partial}{\partial\tau} - \mathrm{i}\alpha U_H(z)\right]\tilde{v} - \frac{1}{Re}\left[\frac{\partial^2}{\partial z^2} - \alpha^2 - \beta^2\right]\tilde{v} - \mathrm{i}\beta\tilde{p} = 0, \tag{3.11}$$

$$\left[\frac{\partial}{\partial\tau} - \mathrm{i}\alpha U_H(z)\right]\tilde{w} - \frac{1}{Re}\left[\frac{\partial^2}{\partial z^2} - \alpha^2 - \beta^2\right]\tilde{w} - \frac{\partial\tilde{p}}{\partial z} + \frac{\partial U_H}{\partial z}\tilde{u} + N\tilde{w} - \mathrm{i}\alpha\tilde{\phi} = 0, \tag{3.12}$$

$$\mathrm{i}\alpha\tilde{u} + \mathrm{i}\beta\tilde{v} + \frac{\partial\tilde{w}}{\partial z} = 0, \tag{3.13}$$

$$\left[\frac{\partial^2}{\partial z^2} - \alpha^2 - \beta^2\right]\tilde{\phi} + N\frac{\partial\tilde{u}}{\partial z} - \mathrm{i}\alpha N\tilde{w} = 0 \tag{3.14}$$

with the boundary conditions

$$\tilde{u} = \tilde{v} = \tilde{w} = 0, \quad \frac{\partial\tilde{\phi}}{\partial z} = 0 \quad \text{at } z = \pm 1. \tag{3.15}$$

The symbol τ denotes $\tau \equiv -t$. This relation means that the equations should be solved backwards in time. One obtains the optimal perturbation for time T by using an iterative scheme which propagates a given initial condition forward in time using the direct problem, the result of which serves as an 'initial' condition for the backward propagation by the adjoint equations. After one forward–backward integration an updated initial condition for the next iterative step is available. Convergence is reached when the initial condition for the forward problem does not change appreciably – up to a normalization constant – by an appropriately chosen criterion from one iterative step to the next. The maximum energy amplification $\hat{G}(\alpha, \beta, T, Re, Ha)$ is then obtained by propagating the converged initial condition forward in time and by computing the ratio $E(T)/E(0)$.

The direct and adjoint equations are solved numerically using a pseudospectral method based on Chebyshev polynomials and a projection approach to enforce incompressibility. The code is based on the one used by Schmid & Rossi (2004) and has been adapted to the MHD channel flow.

4. Linear evolution results

In the pure hydrodynamic channel flow problem ($Ha=0$), the linear optimal growth has been thoroughly investigated in the literature (see e.g. Butler & Farrell 1992). It has been found that, below the linear instability threshold, the maximum transient amplification is achieved by streamwise vortices ($\alpha=0$) evolving into

† Details are contained in an Appendix available with the online version of the paper.

streamwise streaks due to the lift-up process, while purely spanwise two-dimensional modes ($\beta = 0$) experience minor amplification via the Orr mechanism. Hereafter the latter mode wil be referred to as the two-dimensional Orr mode or simply the Orr mode.

In this section, we investigate how the transient growth changes in the presence of a spanwise magnetic field. We first analyse the effect of magnetic field on the streamwise vortices. Thereafter, the case of oblique modes of arbitrary orientation is considered. A wide range of Hartmann numbers is investigated, while the Reynolds number is kept at $Re = 3000$ or $Re = 5000$, chosen as the values which are below the instability threshold and have received close attention in the previous investigations of the non-magnetic case.

The search for optimal perturbations is performed in a square (α, β)-domain (a β-interval in the case of streamwise perturbations) with the wavenumbers varying from 0 to 4. Our calculations have shown that this range is sufficient to determine the global maximum, except for very small times T, when the amplification is low anyway. It should be mentioned that, owing to the symmetries of the governing equations and boundary conditions, only the quadrant with positive α and β need be considered. The growth and amplification at symmetric (α, β) in other quadrants are identical. The number of Chebyshev polynomials used in the vertical direction is 64; to ensure that this is sufficient we have verified all the maxima with 128 polynomials, with obtained differences being under 1 %.

The iterative method described in the previous section computes the maximum energy amplification $\hat{G}(\alpha, \beta, T, Re, Ha)$ which is provided by the optimal z-dependence of a perturbation of specific α, β, T, Ha, Re. This function itself can be maximized over α and β to provide $\hat{M}_{tot}(T, Re, Ha)$ – the maximum amplification among all the perturbations at given time T and flow parameters. This maximum amplification $\hat{M}_{tot}$ is reached at particular wavenumbers α and β depending on the parameters (T, Re, Ha). Further maximization over time T provides the global maximum amplification $M_{tot}(Re, Ha)$ which is reached at time $T = T_{opt}(Re, Ha)$. The corresponding optimal wavenumber pair is denoted by $(\alpha_{opt}(Re, Ha), \beta_{opt}(Re, Ha))$. For the purely streamwise perturbations, when the function $\hat{G}(\alpha, \beta, T, Re, Ha)$ is maximized over β keeping $\alpha = 0$, equivalent optimal quantities may be defined. They are denoted by $\hat{M}_{stream}(T, Re, Ha)$, $M_{stream}(Re, Ha)$ and $\beta_{stream}(Re, Ha)$.

4.1. *Streamwise perturbations*

The results obtained for streamwise perturbations are summarized in figure 1. The effect of the magnetic field is two-fold. First, the transient growth is strongly suppressed by the imposed magnetic field (see figure 1*a*). The maximum amplification $M_{stream}(Re, Ha)$ decreases with Ha, so that no appreciable amplification is present at $Ha \geqslant 100$. Second, the structure of optimal modes is affected. The principal pattern of the evolution of the perturbations (streamwise vortices evolving into streamwise streaks) remains the same as in the non-magnetic case. The spatial shape of the optimal modes is, however, changed by the magnetic field. It is shown in figure 1(*b*) and further illustrated in figure 2 that the spanwise wavenumber $\beta_{stream}(Re, Ha)$ decreases with Ha. The optimal modes become increasingly elongated in the spanwise direction according to the tendency of the imposed magnetic field to suppress the flow gradients in its direction. By contrast, the wavenumber β_{stream} depends only slightly on the Reynolds number.

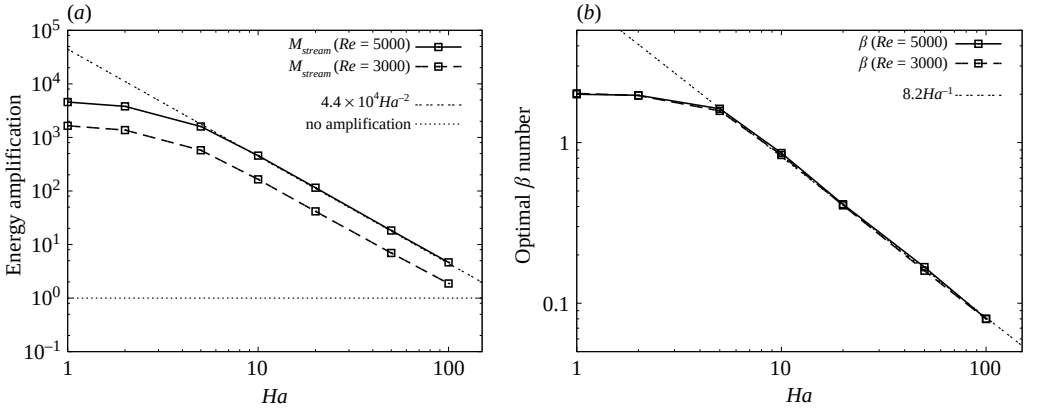

FIGURE 1. Maximum amplification $M_{stream}(Re, Ha)$ (*a*) and optimal $\beta_{stream}(Re, Ha)$ (*b*) as functions of Hartmann number Ha for two subcritical Reynolds numbers $Re = 3000$ and 5000.

As Ha increases, β_{stream} reaches the lower limit set by the grid resolution in β, equal to the grid size ≈ 0.08. This occurs at $Ha = 100$ in our calculations. Since this mode displays almost no amplification we do not refine the grid any further.

It is evident from figures 1(*a*, *b*) that the maximum amplification factor $M_{stream}(Re, Ha)$ and the corresponding optimal wavenumber $\beta_{stream}(Re, Ha)$ follow power-law dependences on Ha in the range $5 < Ha < 100$:

$$M_{stream} \approx Ha^{-2}, \quad \beta_{stream} \approx Ha^{-1}. \tag{4.1}$$

Support (albeit not a proof) for this scaling law can be obtained from an asymptotic analysis of the Orr–Sommerfeld and Squire equations in a way similar to that done for the non-magnetic case (see e.g. Schmid & Henningson 2001). The linear stability equations can be easily written in terms of the Fourier amplitudes of the vertical vorticity component $\hat{\eta} \equiv -\mathrm{i}\beta\hat{u}$ and vertical velocity component $\hat{w}$:

$$\partial_t \hat{\eta} - \frac{1}{Re}(\mathrm{D}^2 - \beta^2)\hat{\eta} = \mathrm{i}\beta\hat{w}\mathrm{D}U - i\beta N\mathrm{D}\hat{\phi} - N\hat{\eta}, \tag{4.2}$$

$$\left[\partial_t - \frac{1}{Re}(\mathrm{D}^2 - \beta^2)\right](\mathrm{D}^2 - \beta^2)\hat{w} = \beta^2 N\hat{w}, \tag{4.3}$$

$$(\mathrm{D}^2 - \beta^2)\hat{\phi} = \frac{\mathrm{i}\mathrm{D}\hat{\eta}}{\beta}, \tag{4.4}$$

where D denotes the partial derivative with respect to z. Let us now introduce scaled variables

$$t' = t/Re, \quad \eta' = \hat{\eta}/(\beta Re), \quad w' = \hat{w}, \quad \Phi' = \hat{\phi}/Re. \tag{4.5}$$

With these scalings, one obtains

$$\partial_t \eta' - (\mathrm{D}^2 - \beta^2)\eta' = \mathrm{i}w'\mathrm{D}U - Ha^2(\mathrm{i}\mathrm{D}\Phi' + \eta'), \tag{4.6}$$

$$[\partial_t - (\mathrm{D}^2 - \beta^2)](\mathrm{D}^2 - \beta^2)w' = \beta^2 Ha^2 w', \tag{4.7}$$

$$(\mathrm{D}^2 - \beta^2)\Phi' = i\mathrm{D}\eta'. \tag{4.8}$$

Differentiating (4.6) and using (4.8), one obtains

$$\partial_t D\eta' - (\mathrm{D}^2 - \beta^2)\mathrm{D}\eta' = \mathrm{i}\mathrm{D}(w'\mathrm{D}U) - \mathrm{i}\beta^2 Ha^2\Phi'. \tag{4.9}$$

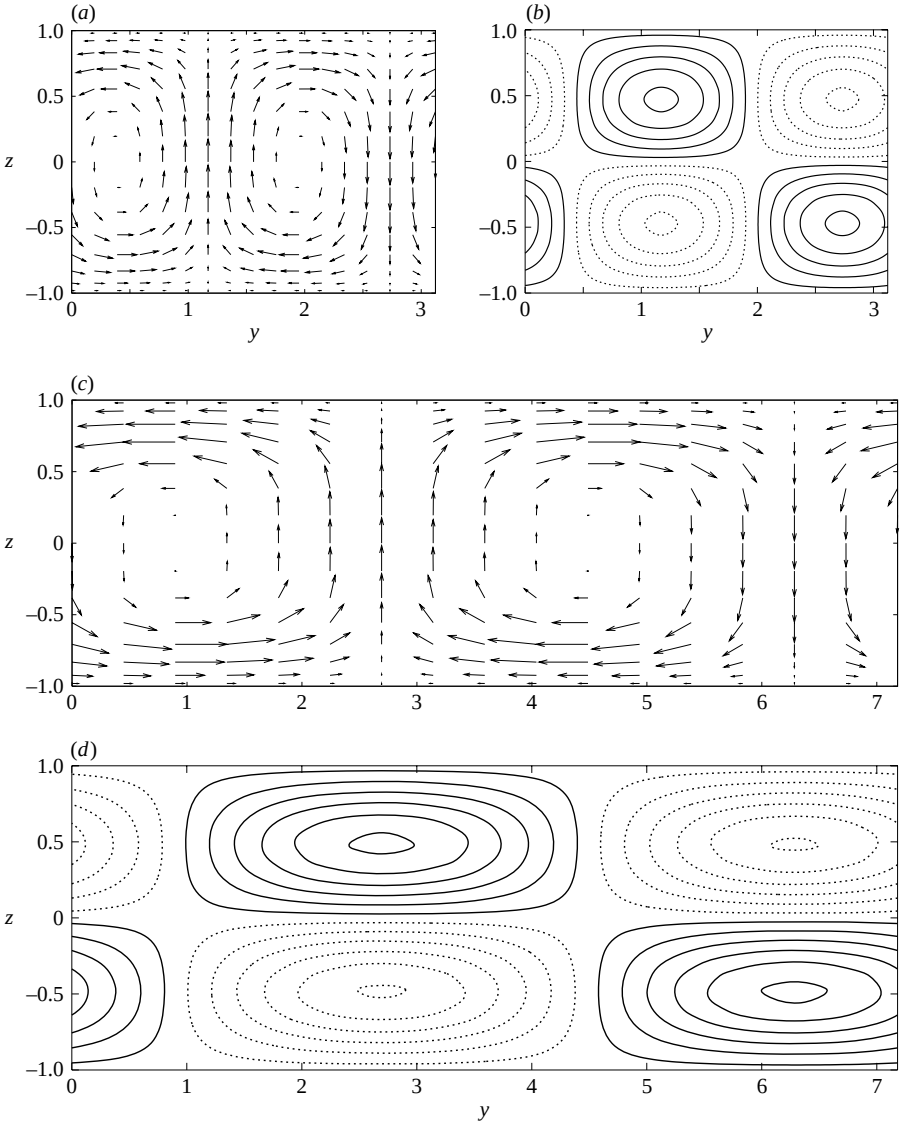

FIGURE 2. The streamwise-independent optimal perturbation which generates the maximum amplification $M_{stream}(Re, Ha)$ for Reynolds number $Re = 5000$ and Hartmann numbers $Ha = 0$ (a, b) and $Ha = 10$ (c, d). (a, c) Projections of the perturbation velocity fields on the (y, z)-plane at the initial time $t = 0$. (b, d) Contours of streamwise velocity at time $t = T_{opt}$, positive and negative values are represented by solid and dotted lines respectively.

Equations (4.7) and (4.9) depend on only two parameters: β^2 and $\beta^2 Ha^2$. In terms of the rescaled variables, the perturbation kinetic energy norm is now

$$E(t) \equiv \frac{1}{\beta^2}(E_{w'}(t) + \beta^2 Re^2 E_{\eta'}(t)) \tag{4.10}$$

with

$$E_{w'}(t) = \int_{-1}^{1} (|\mathrm{D}w'|^2 + \beta^2 |w'|^2)\,\mathrm{d}z \quad \text{and} \quad E_{\eta'}(t) = \int_{-1}^{1} |\eta'|^2\,\mathrm{d}z. \tag{4.11}$$

If we assume that the mechanism of ordinary hydrodynamics applies, in which the growth is due to the forcing of normal vorticity by vertical velocity, the energy at $t=0$ is predominantly in the $E_{w'}$ term and at $t=T$ – or, equivalently, $t'=T/Re$ – predominantly in the $E_{\eta'}$ term. This imposes that

$$\hat{G}(0, \beta, T, Re, Ha) = \beta^2 Re^2 G\left(\frac{T}{Re}, \beta^2, \beta^2 Ha^2\right),$$

where $G(t', \beta^2, \beta^2 Ha^2)$ is a function determined by an optimization problem: find the optimum perturbation in w', η' satisfying (4.7) and (4.9) which maximizes the ratio

$$\frac{E_{\eta'}(t')}{E_{w'}(0)} \tag{4.12}$$

at t'. Let us now assume that β_{stream} tends asymptotically to zero as Ha grows. In that case,

$$\hat{G}(0, \beta_{stream}, T, Re, Ha) = \beta_{stream}^2 Re^2 H\left(\frac{T}{Re}, \beta_{stream}^2 Ha^2\right)$$

where $H(t', R)$ is a function determined by a simplified optimization problem: find the optimum perturbation in w', η' satisfying equations depending on a unique coefficient R:

$$\partial_t \mathrm{D}\eta' - \mathrm{D}^2\mathrm{D}\eta' = \mathrm{i}\mathrm{D}(w'\mathrm{D}U) - \mathrm{i}R\Phi', \tag{4.13}$$

$$[\partial_t - \mathrm{D}^2]\mathrm{D}^2 w' = Rw', \tag{4.14}$$

$$\mathrm{D}^2\Phi' = \mathrm{i}\mathrm{D}\eta', \tag{4.15}$$

which maximizes the ratio (4.12) at t'.

Let us assume that the function $RH(t', R)$ possesses a maximum maximorum at $R=R_c$ and $t'=t'_c$, which can be checked numerically. This is easily seen to imply the following scaling:

$$M_{stream}(Re, Ha) = \frac{Re^2}{Ha^2} R_c H(t_c, R_c), \tag{4.16}$$

$$\beta_{stream} = \frac{\sqrt{R_c}}{Ha} \quad \text{and} \quad T_{opt} = Re\, t'_c. \tag{4.17}$$

In turn, this implies that the scaling (4.1) applies and that curves of the normalized amplification factor

$$\frac{Ha^2}{Re^2}\hat{G}(0, \beta_{stream}(Re, Ha), T, Re, Ha) \tag{4.18}$$

plotted as a function of the normalized time T/Re for different Reynolds and Hartmann numbers nearly collapse onto a single curve. Figure 3 shows that this is observed in our calculations.

4.2. *Perturbations of arbitrary orientation*

Consideration of perturbations of arbitrary orientation reveals the main difference between the magnetic and non-magnetic cases. At Hartmann numbers larger than a low critical value (between 2 and 5 for both values of Re considered) the strongest transient growth is provided by oblique perturbations with $\alpha \neq 0$. Typical behaviour of the amplification factor $\hat{G}$ is illustrated in figures 4 and 5. Isolines of $\hat{G}(\alpha, \beta, T, Re, Ha)$ are shown as functions of α and β at different times T for $Re=5000$ and two Hartmann numbers $Ha=10$ and $Ha=50$. Further information is provided in figure 6

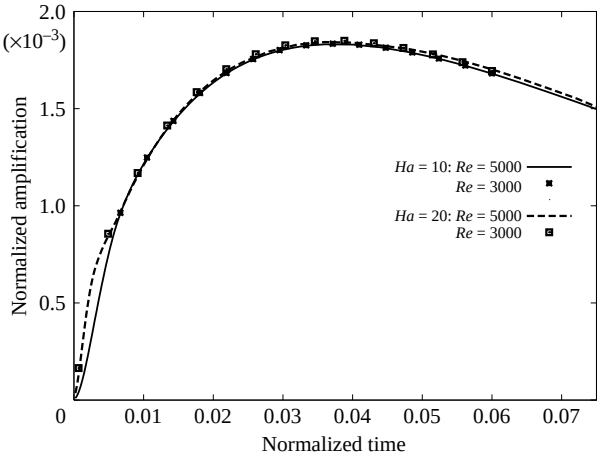

FIGURE 3. The normalized amplification factor $Ha^2/Re^2\hat{G}(0, \beta_{stream}(Re, Ha), T, \mathrm{Re}, Ha)$ as a function of T/Re for the streamwise optimal modes for $Re = 3000$, 5000 and $Ha = 10$, 20.

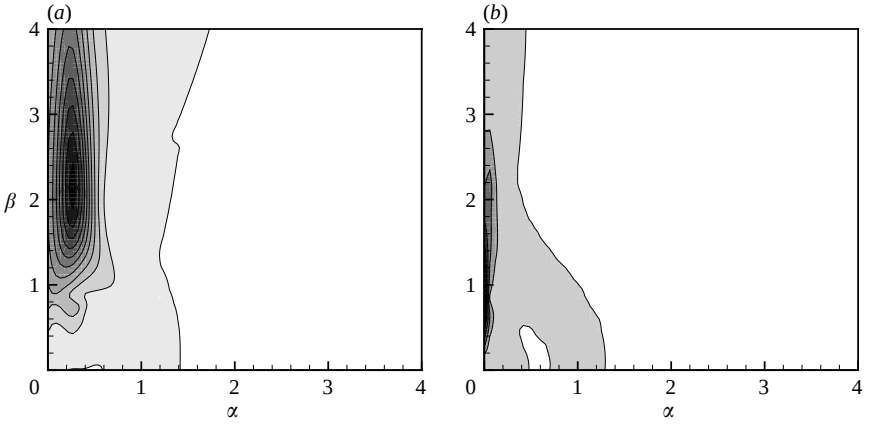

FIGURE 4. Isolines of energy amplification $\hat{G}(\alpha, \beta, T, Re, Ha)$ in the (α,β)-plane for Reynolds number $Re = 5000$ and Hartmann number $Ha = 10$ and for two typical times T (see figure 6*b*). (*a*) $T = T_{opt} \approx 64$, at which the global maximum is reached; (*b*) $T \approx 189$, which corresponds to the optimal time for purely streamwise perturbations.

that shows the maximum amplification $\hat{M}_{tot}(T, Ha, Re)$ and the corresponding values of α and β as functions of T. One can see in figure 6 that the ranges used for α and β are inadequate at very small T. This is of little importance since the amplification levels reached at such T are fairly low.

Data for the non-magnetic case $Ha = 0$ repeat the classical results of Butler & Farrell (1992) and are included in figure 6(*a*) for the sake of comparison. The optimal perturbations are purely streamwise in this case. For $Ha = 10$, which represents the cases of small and moderate Hartmann numbers, there is a single peak of the amplification curve corresponding to an oblique mode at T_{opt} (see figures 4 and 6*b*). For large times T (here $T > 189$), the streamwise perturbations dominate. It should be stressed that the effect of the magnetic field on the spatial shape of optimal perturbations is quite strong even at such a small Hartmann number. The global maximum $M_{tot}(Re, Ha)$ observed for an oblique mode at $T \approx 64$ is about twice

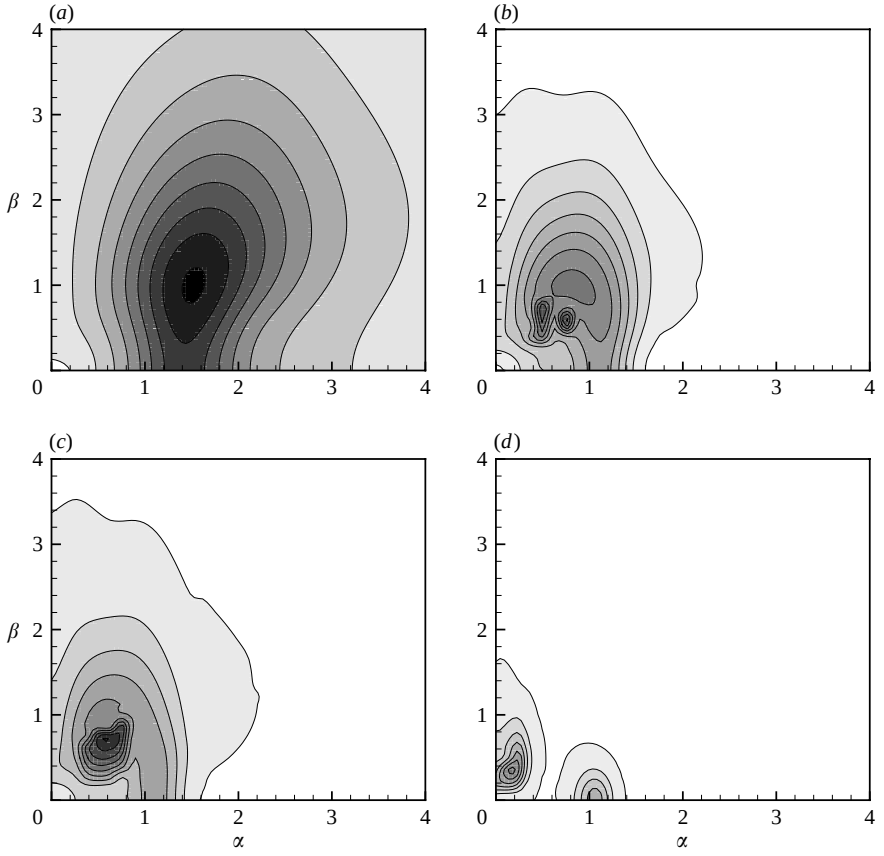

FIGURE 5. Isolines of energy amplification $\hat{G}(\alpha, \beta, T, Re, Ha)$ in the (α,β)-plane for Reynolds number $Re = 5000$ and Hartmann number $Ha = 50$ and for typical times T (see figure 6c). (a) $T = T_{opt} \approx 15$ at which the global maximum is reached, (b) $T \approx 28$ which corresponds to the appearance of two additional local peaks in the (α,β)-plane, (c) $T \approx 33$ and (d) $T \approx 88$ corresponding to the second and third local maxima of the amplification curve in figure 6(c).

the maximum amplification $M_{stream}(Re, Ha)$ obtained at $T \approx 189$ for the streamwise modes.

The picture is more complex at higher Hartmann numbers as illustrated in figures 5 and 6(c) for $Ha = 50$. Again, streamwise modes dominate at large T, but the curve of maximum amplification in figure 6(c) shows three discernible peaks corresponding to the global maximum at $T_{opt} \approx 15$ and two local maxima at $T \approx 33$ and $T \approx 88$, labelled (1), (2), (3). These peaks are associated with the dominance of oblique modes with different streamwise and spanwise wavenumbers. This can also be seen in the evolution of local maxima of the $\hat{G}$ distribution in the (α,β)-plane. An illustration is given in figure 5, which shows the snap-shots corresponding to, respectively, (a) time $T = T_{opt}$ when only one local maximum is present in the (α,β)-plane, (b) $T \approx 28$ when three co-existing local maxima are present, (c) $T \approx 33$ when the local maxima have been replaced by one global maximum, and (d) $T \approx 88$ when a new local maximum appears on the α-axis.

For the case of very strong magnetic fields illustrated by figure 6(d) for $Ha = 100$, the maximum amplification is provided at any T by perturbations with $\beta = 0$. These perturbations take the form of vortices with axes parallel to the magnetic field. Since

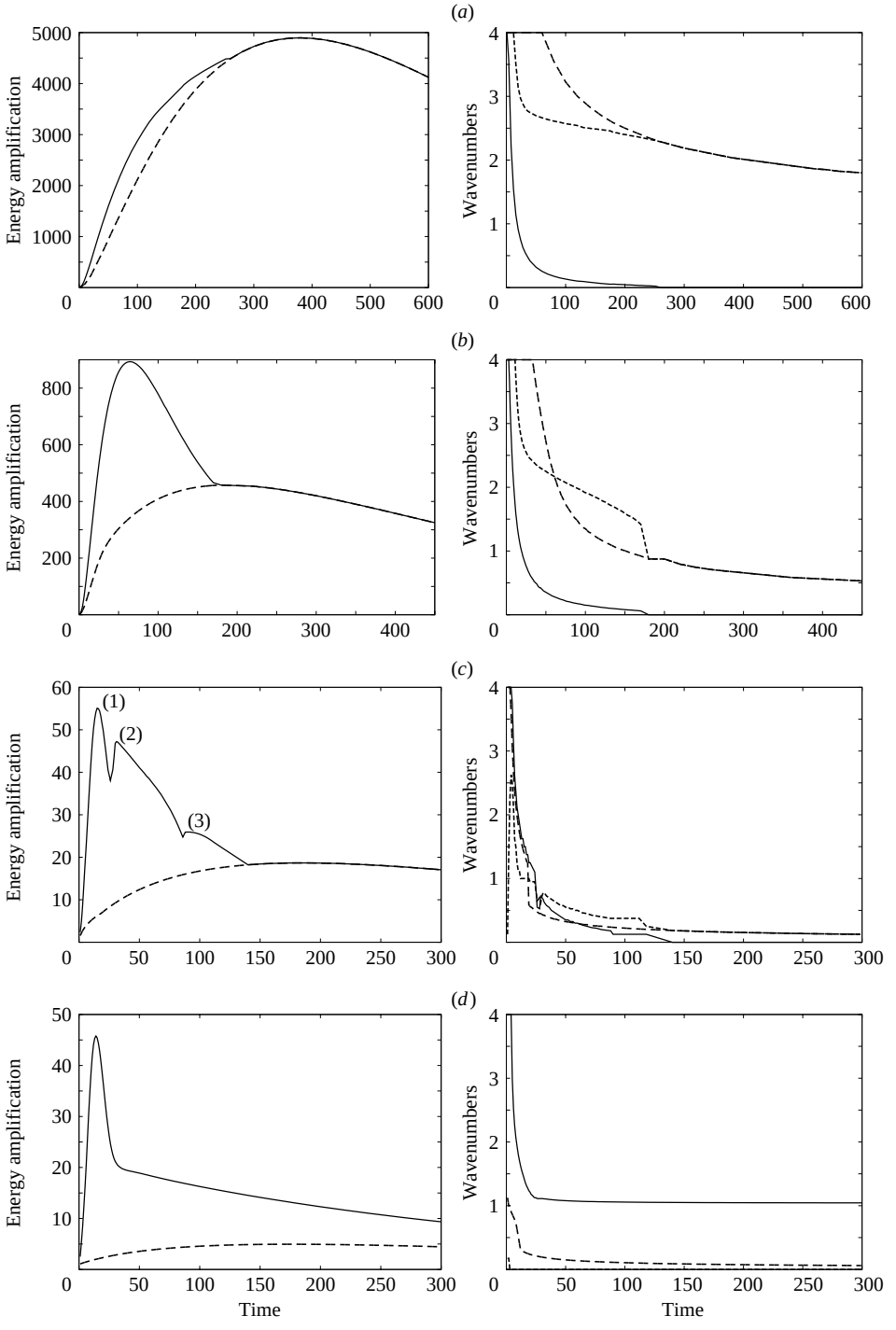

FIGURE 6. On the left, energy amplification factors $\hat{M}_{tot}(T, Re, Ha)$ (—) and $\hat{M}_{stream}(T, Re, Ha)$ (– – – –) as functions of time T. On the right, dominant wavenumbers α (—) and β (- - - -) at which the energy amplification $\hat{M}_{tot}(T, Re, Ha)$ reaches its maximum for a given time T. Dominant spanwise wavenumbers β (– – – –) at which the energy amplification $\hat{M}_{stream}(T, Re, Ha)$ of streamwise modes reaches its maximum for a given time T are also shown. The results presented correspond to $Re = 5000$ and (*a*) $Ha = 0$, (*b*) $Ha = 10$, (*c*) $Ha = 50$, (*d*) $Ha = 100$.

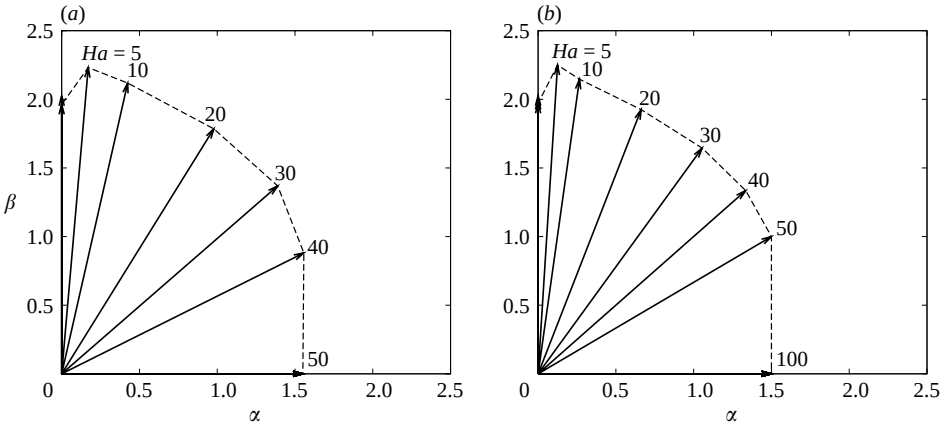

FIGURE 7. Optimal wavevector $(\alpha_{opt}, \beta_{opt})$ vs. Hartmann number Ha for $Re = 3000$ (a) and $Re = 5000$ (b).

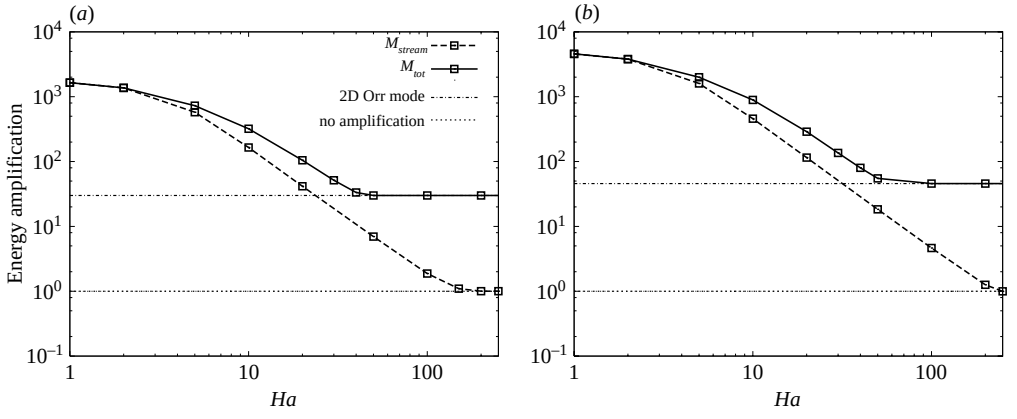

FIGURE 8. Maximum amplification factors M_{tot} and M_{stream} vs. Hartmann number Ha for $Re = 3000$ (a) and $Re = 5000$ (b).

these spanwise modes are unaffected by the magnetic field, their spatial shape and evolution are necessarily identical to those of the spanwise perturbations produced by the two-dimensional Orr mechanism in a purely hydrodynamic channel flow.

The effect of the magnetic field on the transient growth is summarized in figures 7 and 8. The orientation of the optimal wavenumber vector $(\alpha_{opt}, \beta_{opt})$ and the maximum amplification factors M_{tot} and M_{stream} are shown as functions of Ha. These results are presented for two Reynolds numbers: $Re = 3000$ and $Re = 5000$. No principal differences are seen between the two cases. The largest amplification is found for streamwise modes at very small Ha, for oblique modes in a wide range of moderate to large Ha and for spanwise modes at very large Ha. At $Re = 5000$, the range of Ha where oblique modes dominate is larger than at $Re = 3000$.

The oblique modes do not show any discernible scaling with Ha as it was the case for the streamwise perturbations. The amplification factor becomes constant at high Ha, when the dominant modes are purely spanwise modes unaffected by the magnetic field.

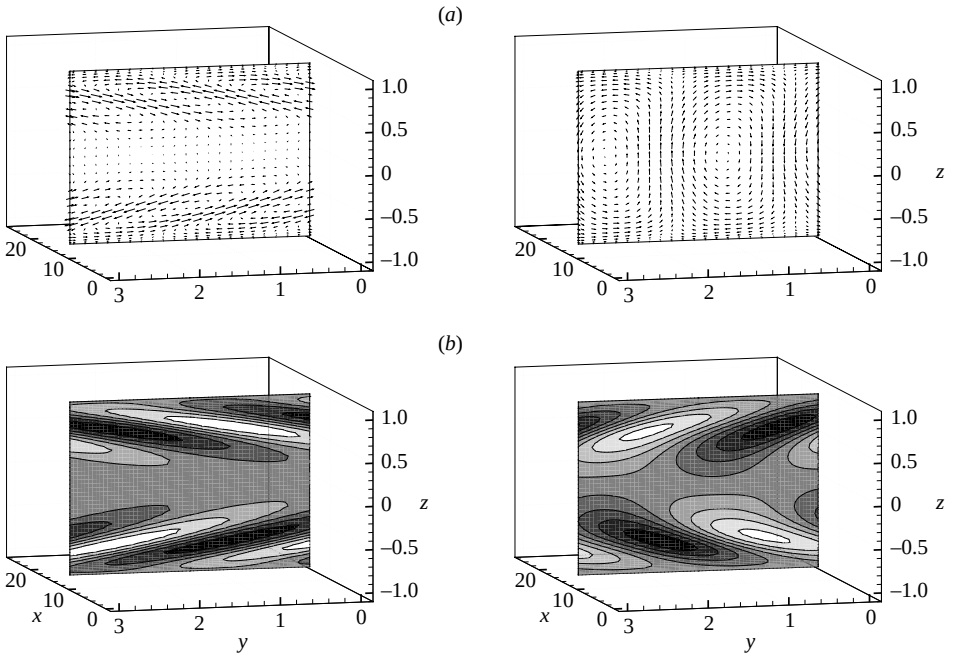

FIGURE 9. The optimal mode corresponding to the maximum amplification $M_{tot}(Re, Ha)$ for $Re = 5000$ and $Ha = 10$. Projections of the perturbation velocity field (*a*) and isolines of streamwise velocity perturbation (*b*) are plotted on a vertical plane parallel to the optimal wavevector $(\alpha_{opt}, \beta_{opt})$ at times $t = 0$ (left) and $t = T_{opt}$ (right).

The projections of the velocity fields and the iso-contours of the streamwise perturbation velocity component upon the vertical plane parallel to the wavenumber vector $(\alpha_{opt}, \beta_{opt})$ are presented in figure 9 for $Ha = 10$. The spatial structure of the initial velocity field of the mode shares some characteristics with the Orr mode (see e.g. Schmid & Henningson 2001), including inclined vortical structures near the walls. On the other hand the optimal mode is clearly not equivalent to the Orr mode, because of its oblique orientation, much stronger amplification and substantial streamwise perturbation velocity component.

Based on a visual inspection of the velocity fields we conclude that the oblique optimal modes cannot be classified as modifications of either Orr modes or classical streamwise vortices. They bear features of both types, although a certain tendency toward increased similarity with the Orr modes is observed as Ha grows. As an example, figure 10 shows the structure of the global optimal mode at $Ha = 50$ and $Re = 5000$. This mode provides the amplification $M_{tot} \approx 55$, which is only slightly higher than the value of 45.7 for the classical Orr mechanism amplification of purely spanwise vortices at the same Re (Butler & Farrell 1992).

The transition between two limiting cases (i.e. purely streamwise and purely spanwise vortices) with growing Ha is illustrated further in figures 11 and 12, which present the vertical profiles of vertical velocity w and vorticity η of the dominant modes for $Ha = 0$, 10, 50 and 100 at the initial time $t = 0$. For example, one can clearly see in figure 11(*c*) that the structure of vertical velocity w for $Ha = 50$ closely follows that of the two-dimensional Orr mode attained at $Ha = 100$ (see figure 11*d*). At the same time, the vertical vorticity η is non-zero at $Ha = 50$ (see right-hand plots in figures 11*c* and 11*d*) since the mode is not two-dimensional. The optimal mode

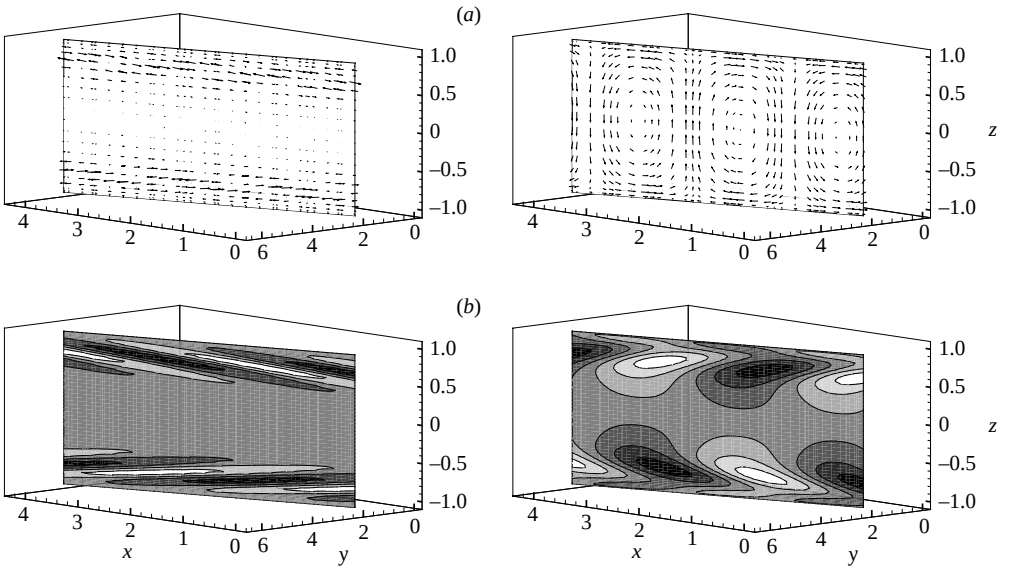

FIGURE 10. The optimal mode corresponding to the maximum amplification $M_{tot}(Re, Ha)$ for $Re = 5000$ and $Ha = 50$. Projections of the perturbation vector field (a) and isolines of streamwise velocity perturbation (b) are plotted on a vertical plane parallel to the optimal wavevector (α_{opt}, β_{opt}) at times $t = 0$ (left) and $t = T_{opt}$ (right).

at $Ha = 10$ (figure 11b) differs from both the Orr mode (figure 11d) and the purely streamwise mode (figure 11a). Comparing the profiles in figures 11(c) and 12(a, b) we see that the oblique modes of different wavelengths, that serve as optimal at different times for $Ha = 50$, also differ significantly in their vertical structure.

A comment can be made regarding the role of oblique modes in the hydrodynamic channel flow. They exist and and possess spatial characteristics similar to those described above. They also experience transient growth, which is stronger than in our magnetic case, but generally weaker than the growth of optimal streamwise modes. Their role in the transition is likely to be indirect, for example via forming a streamwise mode in nonlinear interaction as discussed in the next section.

5. Nonlinear evolution and transition to turbulence

At a subcritical Reynolds number, transient growth of initial perturbations may result in a finite-amplitude modification of the basic velocity profile that is sufficiently strong that the flow becomes unstable to three-dimensional noise. In our problem, the transient growth can be produced by optimal perturbations of different types: streamwise vortices, a single oblique mode, a pair of oblique modes, or spanwise rolls. The same possibilities exist in the non-magnetic case (as discussed by Schmid & Henningson 2001) except that the single oblique mode is never optimal in the linear evolution. The oblique modes may play a role in the transitional behaviour of non-magnetic flows via nonlinear interaction of (α, β) and (α, $-\beta$) modes, which can lead to slightly faster transition than the optimal streamwise modes. The novelty of our case is that the action of the magnetic field renders the oblique and spanwise modes optimal at moderate and high Ha in the sense that they provide the strongest amplification. As discussed below, this also leads to a more important role of the

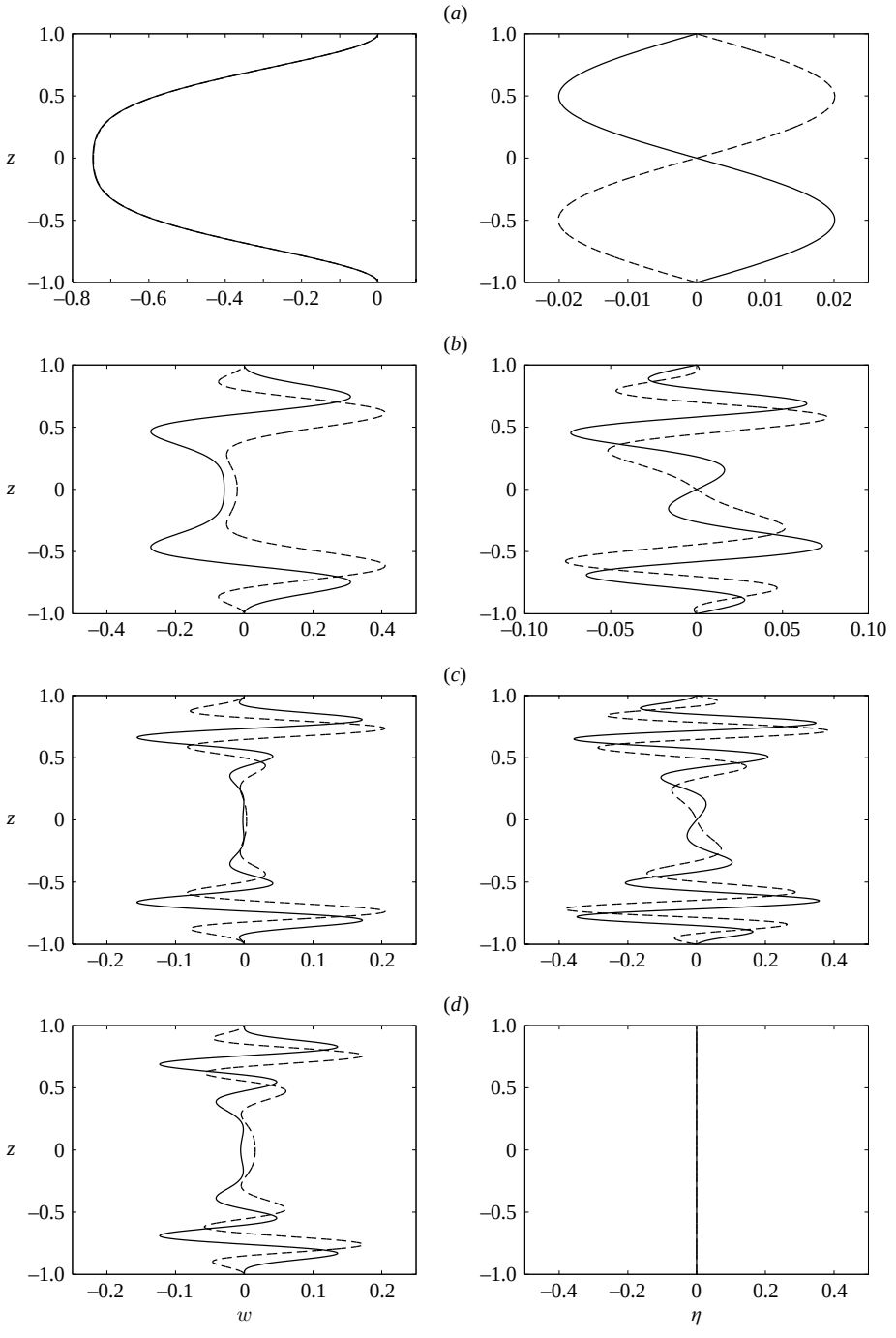

FIGURE 11. The structure of optimal perturbations at the initial state $t = 0$ shown in terms of the real (—) and imaginary (- - - -) parts of the vertical velocity component w (left) and the vertical vorticity η (right). (*a*) The dominant streamwise mode for $Re = 5000$ and $Ha = 0$, (*b*, *c*) the dominant oblique modes for $Ha = 10$, 50 and (*d*) the dominant two-dimensional Orr mode for $Ha = 100$ (see the corresponding maxima in figure 6).

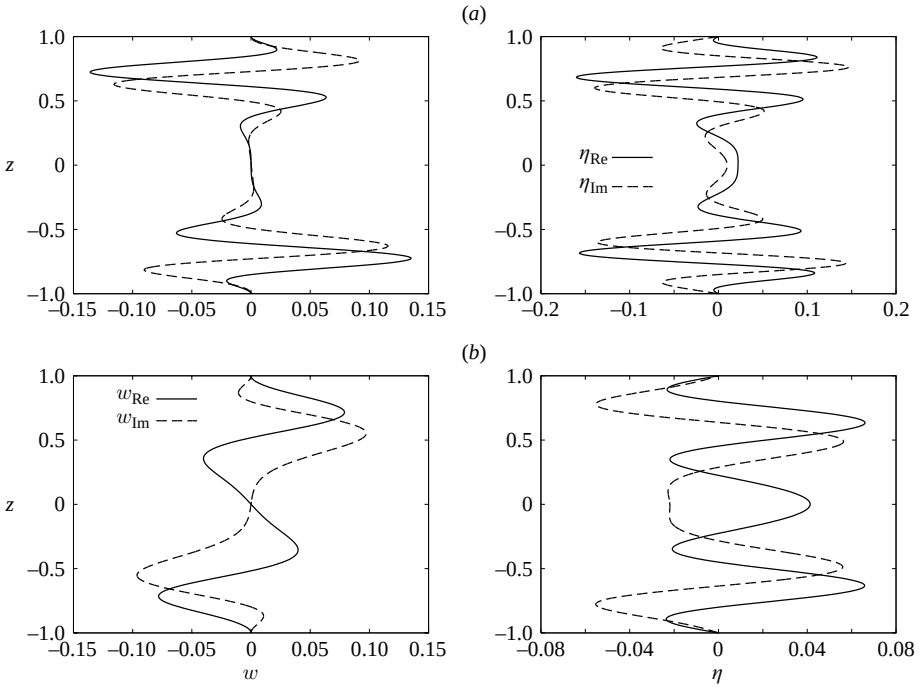

FIGURE 12. The structure of optimal perturbations at the initial state $t = 0$ shown in terms of the real (—) and imaginary (- - - -) parts of the vertical velocity component w (left) and the vertical vorticity η (right). (*a*) The second and (*b*) the third dominant oblique modes for $Re = 5000$ and $Ha = 50$ (see the corresponding maxima in figure 6c).

nonlinear interaction of (α, β) and $(\alpha, -\beta)$ modes, which becomes the most effective mechanism of transition.

We explore the transition to turbulence triggered by the nonlinear evolution of the optimal perturbations previously analysed in the linear context. The representative flow regimes with Ha ranging between 10 and 100 are considered. The initial conditions consist of the basic flow $U_H = 1 - z^2$ modulated by an optimal linear mode of a specified amplitude. The amplitude is chosen so that the kinetic energy of the perturbations $E(0)$ varies between 10^{-5} and 10^{-2} relative to the energy of the basic flow. For cases such as $Ha = 50$, where different linear modes give maximum amplifications at different times, simulations are conducted separately for each such mode used as an initial condition. To trigger the transition, weak three-dimensional noise is added to the modulated flow at the time $t = T_{opt}$ of maximum linear amplification. The energy E_{3D} of the noise is chosen to be 10^{-2} of the initial optimal perturbation energy.

The time at which noise is added can, in principle, be considered as another parameter of the problem since it determines the starting moment and duration of the period during which the secondary instability can evolve. The effect was investigated earlier, for example, by Krasnov *et al.* (2004) for the case of Hartmann flow. It was found that adding the noise before T_{opt} can lead to earlier development of turbulence but no noticeable modification of the process of transition itself. Similar results were obtained in our computations of the flow with spanwise magnetic field. It is important to note that, unless unrealistically strong three-dimensional perturbations are added, the transition always occurs at $t > T_{opt}$. The evolution of the modulated

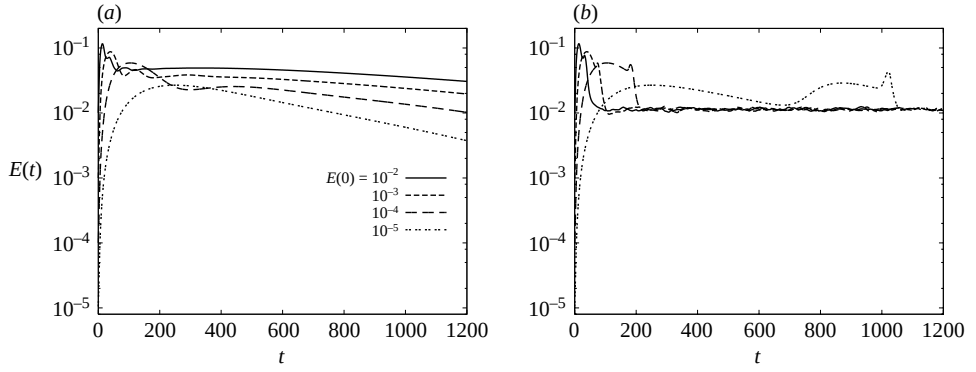

FIGURE 13. The nonlinear evolution of energy $E(t)$ at $Re = 5000$ and $Ha = 0$. The initial energy of the streamwise optimal mode varies from $E(0) = 10^{-5}$ to $E(0) = 10^{-2}$. (*a*) No three-dimensional noise is added, (*b*) noise of energy $E_{3D} = 10^{-2}E(0)$ is added at $t = T_{opt}$.

flow remains largely unaffected by the noise until some time after T_{opt}. Our choice of T_{opt} as the time at which noise is added seems, therefore, pertinent. The effect of three-dimensional perturbations existing in the flow at earlier times is, to some degree, modelled by variation of the noise amplitude.

We numerically simulate the full equations (2.6)–(2.9) using a pseudospectral algorithm and a representation of the flow field in terms of velocity potentials complying with the incompressibility constraint. A detailed description of the method is given in the Appendix.

All simulations are performed with a numerical resolution of 128^3 collocation points in the x-, y- and z-directions. The periodicity lengths are specified as $L_x = 2\pi/\alpha_{opt}$ and $L_y = 2\pi/\beta_{opt}$, where α_{opt} and β_{opt} stand for the optimal wavenumbers found in the linear problem. In case of α_{opt} or β_{opt} equal to 0, i.e. purely spanwise or streamwise perturbations, the corresponding periodicity length is set to 2π.

5.1. *Transition caused by streamwise and oblique modes*

In this section we analyse the transition to turbulence caused by growing oblique and streamwise modes. Special attention is given to the efficiency of these modes in generating the transition. The spanwise modes are discussed in § 5.2 as a separate case.

In the case of oblique rolls, the symmetry of the problem provides a new interesting opportunity. The modes with wavenumbers (α, β) and $(\alpha, -\beta)$ are equivalent solutions of the linearized equations (3.3)–(3.8) with the ansatz (3.2) up to the substitution $\hat{v} \to -\hat{v}$ and have, thus, the same linear transient growth. Their nonlinear interaction might lead to faster transition to turbulence than in the case when only one set of rolls is used. In order to test this possibility, simulations are conducted for different types of initial conditions: a single roll or a superposition of symmetric oblique rolls of equal or different amplitudes.

In the hydrodynamic limit $Ha = 0$, the linear analysis gives the maximum linear amplification $M_{tot}(Re = 5000, 0) \approx 4897$ for the purely streamwise vortices with $(\alpha_{opt}, \beta_{opt}) = (0, 2.04)$ and 45.7 for the Orr mode with $\alpha = 1.48$ (Butler & Farrell 1992). The nonlinear evolution of the streamwise modes is displayed in figure 13, indicating that a perturbation energy of streamwise vortices of $E(0) = 10^{-5}$ and the noise energy $E_{3D} = 10^{-2}E(0)$ is sufficient to trigger the transition.

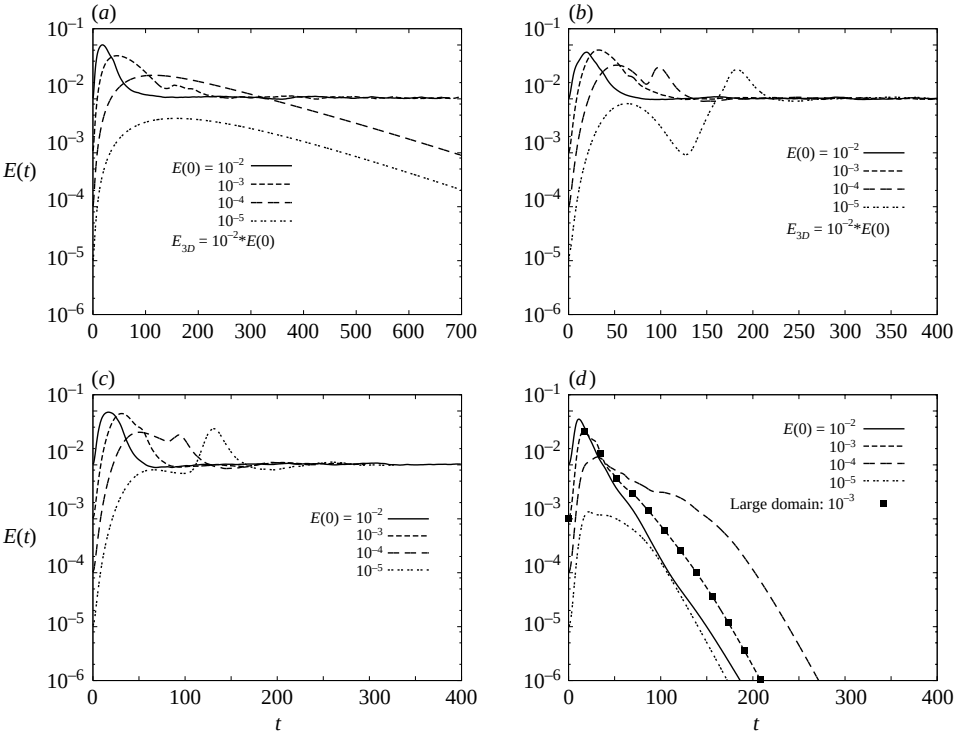

FIGURE 14. The nonlinear evolution of perturbation energy $E(t)$ at $Re = 5000$: (*a*) $Ha = 10$ starting with the streamwise optimal mode, (*b*) $Ha = 10$ starting with a single optimal oblique mode, (*c*) $Ha = 10$ starting with a superposition of two symmetric oblique modes (α,β) and $(\alpha,-\beta)$ of equal amplitudes, (*d*) $Ha = 30$ starting with two symmetric oblique modes of equal amplitude. Initial energy of optimal modes varies from $E(0) = 10^{-5}$ to $E(0) = 10^{-2}$, the three-dimensional noise of energy $E_{3D} = 10^{-2}E(0)$ is added at $t = T_{opt}$ in cases (*a*) and (*b*). For the initial conditions with two symmetric oblique modes, adding three-dimensional noise is unnecessary (see text).

For $Ha = 10$, the linear analysis gives the maximum amplification $M_{tot} \approx 900$ for the oblique modes and $M_{stream} \approx 450$ (at larger T) for the streamwise modes (see figure 6*b*). The corresponding results of direct numerical simulations displayed in figure 14 demonstrate that even at such a modest Hartmann number there is already a significant effect of the magnetic field upon the streamwise vortices. As can be seen in figure 14(*a*), a perturbation energy larger than or equal to 10^{-3} is necessary to induce transition to turbulence. This should be compared with the case $Ha = 0$, where $E(0) = 10^{-5}$ is sufficient. The nonlinear evolution of an oblique optimal mode is similar, except that it is a far better candidate to modulate the flow and trigger the transition. Even an initial energy as small as $E(0) = 10^{-5}$ is sufficient for the transition when three-dimensional noise is added (see figure 14*b*). The transition itself seems to occur earlier than in the case of streamwise vortices. For both streamwise and oblique modes, the flow remains laminar and returns to the basic state if no three-dimensional noise is present, in agreement with the transient character of their growth.

Analysing the flow evolution caused by two superimposed oblique waves with (α,β) and $(\alpha,-\beta)$ (see figure 14*c*) we found transition to turbulence for all $E(0)$ in a range from 10^{-5} to 10^{-2}. The major difference with the one-wave case is that no three-dimensional noise has to be added. Each of the modes plays the role of a

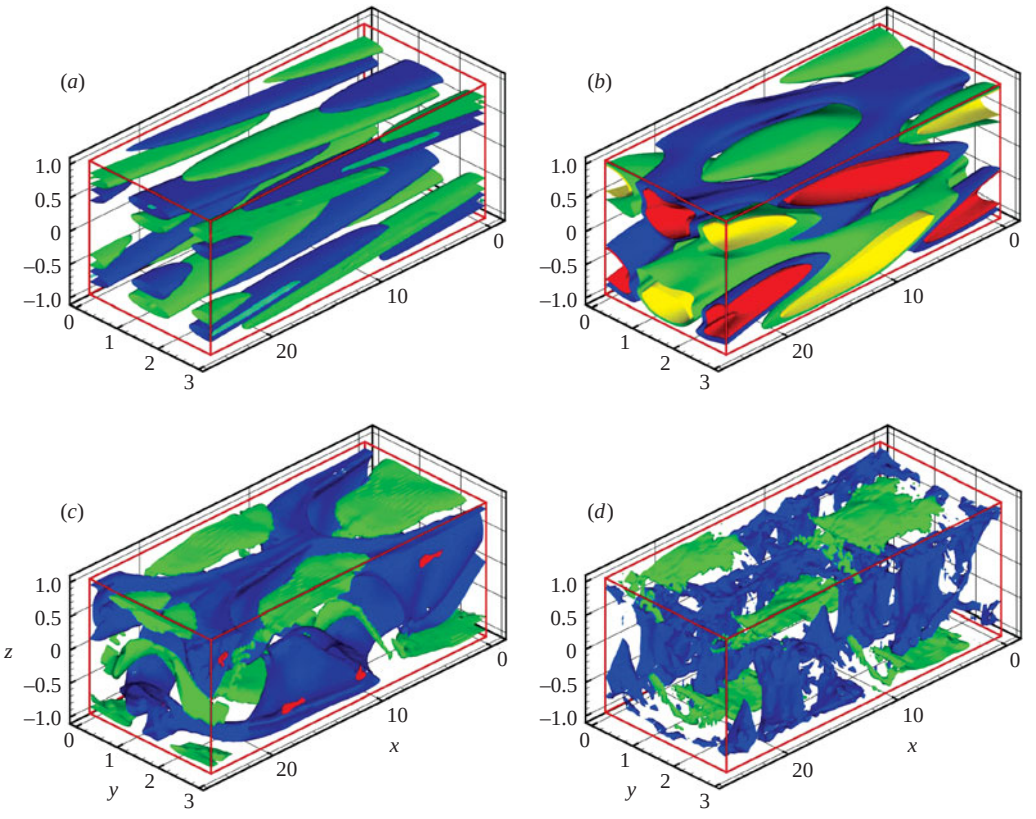

FIGURE 15. Instability and transition to turbulence at $Re = 5000$ and $Ha = 10$ triggered by a superposition of (α, β) and $(\alpha, -\beta)$ optimal perturbations of equal amplitude. Four stages of the evolution are visualized by the isosurfaces of the streamwise velocity perturbations: (*a*) initial state, (*b*) $t \approx 0.33T_{opt}$, (*c*) $t \approx 1.27T_{opt}$, (*d*) $t \approx 1.42T_{opt}$. The isosurfaces correspond to $\pm 45\,\%$ and $\pm 90\,\%$ levels of the maximum amplitude.

secondary perturbation for the other. Nonlinear interaction leads to excitation of the horizontal Fourier harmonics other than the initial two modes. The flow becomes essentially three-dimensional at the early nonlinear stages of the transition. This is illustrated in figure 15, which shows a series of intermediate stages including the initial state, interaction between the two initial oblique modes, breakdown of the growing structures, and, finally, a state preceeding turbulent flow.

In order to further investigate which kind of initial condition is more efficient in triggering the transition, we conducted simulations at $Ha = 10$ and $Re = 5000$ using one oblique mode or two modes of equal or significantly different amplitudes (in the latter case, one amplitude was 10 % of the other). No appreciable differences were found in the characteristics of the developed turbulent state and in the amplitude of perturbations needed to initiate the transition. Some variations were observed in the behaviour during the nonlinear phase of the transient growth. As illustrated in figure 16, the 2-mode solution demonstrates somewhat stronger amplification (approximately a 10 % larger amplification factor G) than the two other solutions. An explanation is also provided in figure 16. The nonlinear interaction between the growing oblique modes (α, β) and $(\alpha, -\beta)$ results in the activation of the Orr mode $(2\alpha, 0)$. One can see

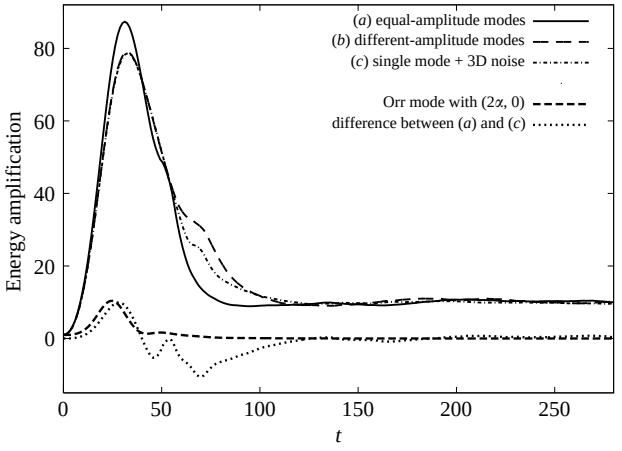

FIGURE 16. The amplification factor $\hat{G}$ of the perturbation energy $E(t)$ at $Re = 5000$ and $Ha = 10$ and different initial modulations of the flow. (a) (—), superposition of two symmetric oblique modes with equal initial amplitudes, (b) (- - -), superposition of two symmetric oblique modes with significantly different initial amplitudes; (c) (.....), single (α,β) oblique mode perturbed by random three-dimensional noise at $t = T_{opt}$. - - - -, Energy of the two-dimensional Orr mode (2α,0) activated in the result of nonlinear interaction of the symmetric oblique modes in case (a). ....., The difference between curves (a) and (c). Initial amplitude of perturbations is $E(0) = 10^{-3}$ in all cases.

that the modest transient growth experienced by this mode accounts almost entirely for the enhanced amplification of the 2-mode solution.

No transition to turbulence was detected at $Ha = 30$ and at higher Hartmann numbers (see figure 14d). We have checked this for all families of optimal linear modes, each providing the maximum amplification in a certain time range and every method of flow excitation (single mode plus three-dimensional noise, superposition of symmetric oblique modes and, additionally, superposition of symmetric oblique modes plus three-dimensional noise). The nonlinear effects become noticeable when the initial perturbation energy exceeds 10^{-3} but the transition to turbulence is never triggered. The possible explanation is two-fold. First, the maximum transient energy amplification is weak (for example, only $M_{tot} \approx 55$ for $Ha = 50$). Furthermore, the Joule dissipation strongly suppresses the three-dimensional perturbations once they are introduced. To conclude this part of the study, we have conducted a series of simulations for $Ha = 30$ and 50 aimed at investigating the possible effect of the size of computational domain on the observed transition. In particular, we wanted to see whether the absence of transition at high Ha is an artefact due to the use of the domain that includes only one wavelength of the optimal mode in the x- and y-directions. The domain was enlarged by factor of 2 in both directions. The number of Fourier modes was doubled as well to maintain the same grid spacing. We have found no major difference with the results obtained in the smaller domain. As an illustration, perturbation energy values calculated in the large domain at $Ha = 30$ are shown in figure 14(d).

5.2. *Transition caused by Orr modes*

At high Hartmann numbers, the transient amplification provided by the Orr modes is comparable to or even stronger (at $Ha \geqslant 100$, see figure 7) than the amplification by the oblique and streamwise modes. It is tempting to consider the Orr modes

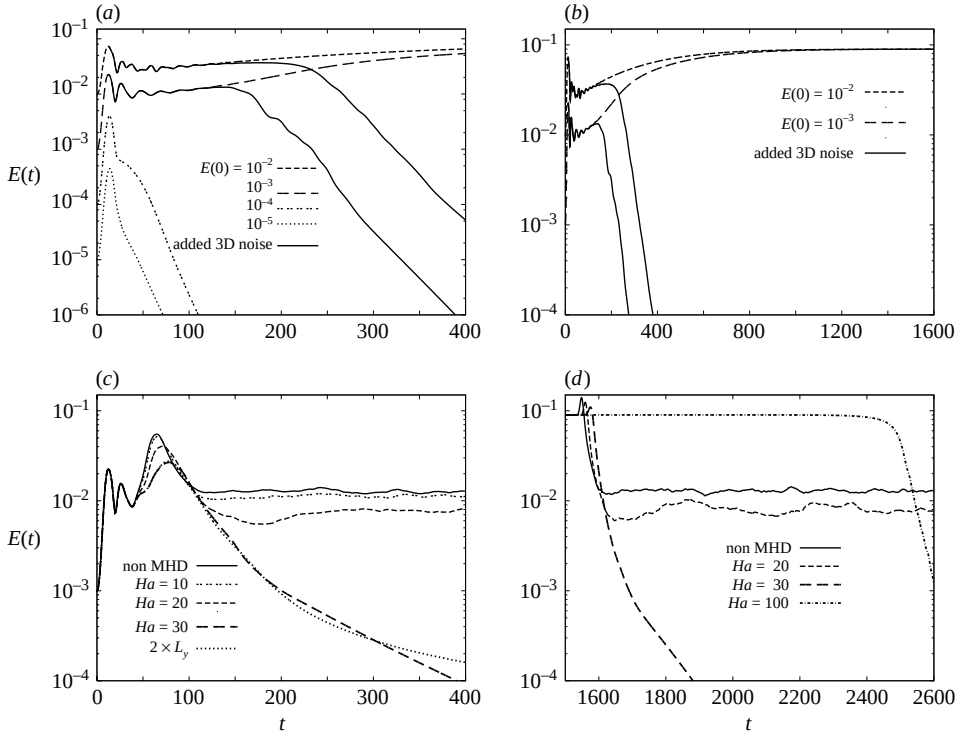

FIGURE 17. The nonlinear evolution of perturbation energy $E(t)$ starting with an Orr mode at $Re = 5000$ and different Ha. (a) $Ha = 100$, the early stage ($t \leqslant 400$) with initial energy $E(0) = 10^{-5}$ ... 10^{-2} and three-dimensional noise of energy $E_{3D} = 10^{-2}E(0)$ added at $t = T_{opt}$ for the solid curves. (b) Case $Ha = 100$, the complete evolution ($t \leqslant 1600$) up to a sustained two-dimensional finite-amplitude state for $E(0) = 10^{-2}$ and 10^{-3}, three-dimensional noise of energy $E_{3D} = 10^{-2}E(0)$ is added at $t = T_{opt}$ for the solid curves. (c) Transition for $0 \leqslant Ha \leqslant 30$ and an initial Orr mode of energy $E(0) = 10^{-3}$, three-dimensional noise of energy $E_{3D} = 10^{-2}E(0)$ is added at $t = T_{opt}$. (d) Instability of the sustained two-dimensional state and transient evolutions for $0 \leqslant Ha \leqslant 100$, three-dimensonal noise of amplitude $E_{3D} = 10^{-7}E_{2Dstate}$ is added at $T \approx 1500$. Curves at $Ha = 0,\ 20,\ 30,\ 100$ are presented.

unaffected by the magnetic field as a possible route to turbulence. Their nonlinear growth and saturation at Reynolds numbers as high as $Re = 5000$ can modify the basic flow to a degree sufficient to make it unstable to three-dimensional noise. On the other hand, the three-dimensional evolution would be strongly suppressed by the magnetic field.

We conducted numerical experiments at $Ha = 100$. The dominant optimal mode, which is an Orr mode in this case, takes the form of purely spanwise vortices (see figure 6d). Sufficiently strong initial perturbations (e.g. $E(0) \geqslant 10^{-3}$ in figure 17(a, b) evolve into a purely two-dimensional finite-amplitude state characterized by oscillations observed earlier by Jimenez (1990) in a two-dimensional non-magnetic channel flow. This evolution can be regarded as a common solution for all values of Ha, including the non-magnetic case. If three-dimensional noise is added at $t = T_{opt}$ in the non-magnetic case (see figure 17c), the transition to a three-dimensional turbulent state is triggered. On the contrary, the noise destroys the time-dependent two-dimensional flow for $Ha = 100$ in such a way that it returns to the basic flow regime as illustrated in figure 17(a, b) (solid curves) and figure 18. We attribute this

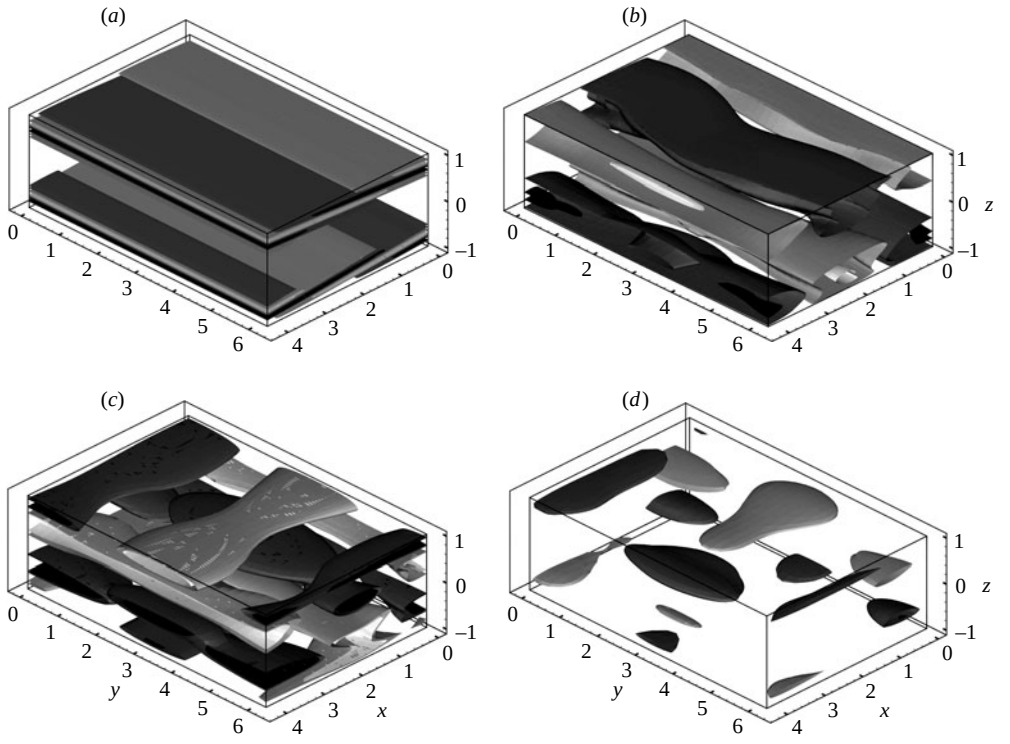

FIGURE 18. Instability and return to the base state at $Re = 5000$ and $Ha = 100$. The simulation is started with the Orr mode as initial condition and three-dimensional noise added at the time of maximum growth. Four stages of the evolution are visualized by the isosurfaces of the streamwise velocity perturbations: (*a*) initial state, (*b*) $t \approx 10T_{opt}$, (*c*) $t \approx 15T_{opt}$, (*d*) $t \approx 18T_{opt}$. The isosurfaces correspond to $\pm 30\,\%$, $\pm 60\,\%$ and $\pm 90\,\%$ levels of the maximum amplitude.

re-laminarization to energy transfer by nonlinear interactions from the two-dimensional modes to three-dimensional modes with a finite spanwise wavenumber, which are rapidly damped by the Joule dissipation. We varied the amplitude E_{3D} and found that even very small noise with $E_{3D} = 10^{-20}E(0)$ (comparable with the round-off error of floating-point operations) is sufficient to trigger the re-laminarization.

Similar simulations were conducted in the entire range $0 \leqslant Ha \leqslant 100$. A re-laminarization similar to that for $Ha = 100$ was found at $Ha \geqslant 30$ (see figure 17*c*, *d*). Transition to turbulence was found at lower Ha (e.g. at $Ha = 10$ and 20). At such Hartmann numbers, transition was also produced by the oblique modes. We can conclude that, although the Orr modes are capable of producing transition to turbulence in the presence of the magnetic field, they are unlikely to play the role of the sole route to turbulence at high Ha.

One has to be careful drawing conclusions based on the results of simulations conducted with a computational domain of finite length ($L_y = 2\pi$ in our case). It is possible that the maximum Hartmann number, at which the transition can occur, is higher if longer (thus, not so strongly magnetically suppressed) spanwise waves are included. To address this issue we have conducted several additional simulations for $Ha = 30, 100$ in a domain with doubled spanwise length L_y as well as the number of modes N_y in the spanwise direction. One of these runs performed for $Ha = 30$ and

initial energy of the Orr mode $E(0) = 10^{-3}$ is shown in figure 17(*c*). One can see that the flow still returns to the laminar state, although the evolution of the perturbation energy differs slightly from that observed in a smaller computational domain. The results indicate that doubling the spanwise wavelength does not significantly affect the transition. Different behaviour is possible at larger wavelengths, which deserves a separate investigation.

Another interesting aspect of the results obtained at $Ha = 100$ is related to whether purely two-dimensional turbulence can be sustained by a strong imposed magnetic field. One possible way forward is to question whether the two-dimensional states are stable to three-dimensional perturbations in the presence of the magnetic field and, if unstable, towards which flow regime they evolve. We do not attempt to fully resolve this intricate and important question but rather provide a counter-example. Two simulations (with $E(0) = 10^{-3}$ and $E(0) = 10^{-2}$) were continued as two-dimensional until the non-steady saturated two-dimensional solutions similar to those found by Jimenez (1990) were obtained (see figure 17*b*). Adding three-dimensional noise at this stage led to the instability of the two-dimensional structures (curves for $Ha = 30$ and 100 in figure 17*d*) and quick energy drain into three-dimensional perturbations, which were then suppressed by the magnetic field. The flow evolved back to the basic state. Interestingly, this happened more slowly in the case of higher Hartmann number ($Ha = 100$). The stronger magnetic field slowed down the growth of the three-dimensional perturbations, and thereby delayed the nonlinear interaction and energy transfer from two-dimensional to three-dimensional structures.

As a general conclusion we state that whereas a sufficiently strong magnetic field eventually suppresses any three-dimensionality in the flow, it cannot sustain the non-steady two-dimensional solutions found by Jimenez (1990).

6. Conclusions

In this paper, we investigate the change of stability properties and the transition to turbulence in a plane channel flow of an electrically conducting fluid in the presence of a uniform constant magnetic field in the spanwise direction. The case of small magnetic Reynolds number is considered. The scenario of transition based on the transient growth of certain perturbations and subsequent secondary instability of the modified base flow was analysed using linear and nonlinear computational models. In the linear part, conducted for subcritical values of the Reynolds number $Re = 3000$ and $Re = 5000$, the optimal (with strongest transient growth) perturbations were determined with the help of the iterative procedure based on integration of direct and adjoint equations. The nonlinear evolution of the optimal modes, their breakdown, and transition to turbulence were investigated in a series of direct numerical simulations for $Re = 5000$.

We found that the magnetic field has strong quantitative and qualitative effects on the transient growth. By means of added Joule dissipation, it reduces the growth of all perturbations except purely spanwise modes. For the streamwise rolls that appear as optimal perturbations in the classical hydrodynamic flow, the suppression is described by power-law dependences with the energy amplification and spanwise wavenumber of the strongest growing mode scaling as Ha^{-2} and Ha^{-1}, respectively.

More interestingly, the preferential suppression of the spanwise velocity gradients by the magnetic field leads to the fact that the orientation of the optimal modes changes under the impact of the magnetic field. At Hartmann numbers above a moderate threshold value (between 2 and 5, depending on the Reynolds number), the

optimal perturbations change from streamwise to oblique rolls. Their oblique angle increases monotonically with Ha, demonstrating the shifting balance between the two opposing energy fluxes: the Joule dissipation and the energy transfer from the basic flow, both of which decrease with the growing oblique angle. At sufficiently strong magnetic field characterized by Ha larger than a threshold between 50 and 100, the strongest (and quite moderate) growth is supplied by purely spanwise Orr modes unaffected by the magnetic field.

In the nonlinear analysis we first focused on the transition to turbulence caused by the breakdown of growing streamwise or oblique modes at Hartmann numbers in the range $5 \leqslant Ha \leqslant 50$. Numerical experiments were conducted, in which linear optimal modes of low amplitude were used as initial conditions and weak three-dimensional noise was added to trigger the secondary instability. It was found that stronger optimal growth of the oblique modes renders them better candidates for the dominant mechanism of the transition. For example, at $Ha = 10$ and $Re = 5000$, an initial energy not less than 10^{-3} of the energy of the base flow is required by the streamwise modes to initiate the transition, while energy levels as small as 10^{-5} are sufficient for the oblique modes.

The oblique orientation of the optimal modes at moderate Ha opens an interesting possibility of simultaneous growth of two superimposed symmetric modes, (α, β) and $(\alpha, -\beta)$. We found that these modes efficiently serve as secondary disturbances for each other so there is no need to add noise to trigger the transition. Nonlinear interaction between the symmetric modes generates other modes experiencing transient growth. In particular, the spanwise mode $(2\alpha, 0)$ was shown to provide approximately a 10 % increase of the total energy amplification of the perturbations.

In the case of strong magnetic fields at Ha about 100 and higher, the spanwise perturbations are the only ones experiencing noticeable transient growth. We found that these modes are unable to generate the transition to turbulence at high Ha. Their growth and nonlinear saturation lead to establishment of a spanwise-independent secondary flow observed earlier in the two-dimensional simulations of Jimenez (1990). Instability of this flow to three-dimensional perturbations cannot be suppressed by the magnetic field in the range of Ha considered in the present paper. The instability leads to the transition back into the base state. Further investigations are needed to resolve interesting related questions, such as that of stability of the two-dimensional solutions at even higher Ha and the role played by the spanwise Orr modes in the transition at supercritical Re.

We would like to comment on the relative importance of lift-up and Orr growth (transient or exponential) mechanisms in the presence of the spanwise magnetic field. The fact that optimal oblique and streamwise modes are damped, while the spanwise Orr modes are not affected, diminishes the possible role played by the lift-up mechanism. On the other hand, we found that the mechanism is active at small and moderate Ha, generating transition at subcritical Reynolds number. At higher Ha, the primary role is played by purely spanwise perturbations growing either transiently or exponentially. One has to take into account, however, that the evolution of such perturbations is unaffected by the magnetic field only as long as they stay two-dimensional. Any development into a three-dimensional turbulent flow would be strongly suppressed by the magnetic field.

We are grateful to André Thess and Peter J. Schmid for interesting discussions and useful comments. T. B. and O. Z. are also grateful to Professor Moin and the staff of the Center for Turbulence Research (CTR) for their hospitality during the 2006 summer

program at Stanford University, where much of this work was performed. T. B., D. K. and M. R. acknowledge financial support from the Deutsche Forschungsgemeinschaft in the framework of the Emmy–Noether Program (grant Bo 1668/2-2). O. Z.'s work is supported by the grant DE FG02 03 ER46062 from the US Department of Energy. Financial support for the collaboration between the TU Ilmenau and the University of Michigan–Dearborn is provided by the Deutscher Akademischer Austauschdienst and the National Science Foundation (grant OISE 0338713). Computer resources were provided by the CTR and the computing centres of TU Ilmenau and of the Forschungszentrum Jülich (NIC).

Appendix. Method of direct numerical simulations

Equations (2.6)–(2.9) are solved using a pseudospectral method based on Fourier series in x and y and a Chebyshev polynomial expansion in z (Canuto *et al.* 1988; Gottlieb & Orszag 1977). The solenoidal velocity field is represented through the poloidal–toroidal decomposition as

$$\boldsymbol{v}(x, y, z, t) = \nabla \times (\nabla \times \boldsymbol{e}_z \varphi(x, y, z, t)) + \nabla \times (\boldsymbol{e}_z \psi(x, y, z, t)). \tag{A1}$$

Equations for the scalar fields φ and ψ are derived by taking respectively the curl and twice the curl of the momentum equation and projection onto the vertical direction. We obtain equations for the vertical velocity $v_z = -\Delta_h \varphi$ and the vertical vorticity $\omega_z = -\Delta_h \psi$, where $\Delta_h = \partial_x^2 + \partial_y^2$ and $\omega = \nabla \times \boldsymbol{v}$ is the vorticity. The quantities v_z and ω_z determine the velocity field up to a mean flow $U(z, t)\boldsymbol{e}_x + V(z, t)\boldsymbol{e}_y$. Equations for U and V are obtained by averaging the momentum equation over horizontal cross-sections of the periodicity domain. The evolution equations based on the poloidal–toroidal representation take the form

$$\nabla^2 \omega_z - Re\, \partial_t \omega_z = F, \tag{A2}$$

$$\nabla^2 \eta - Re\, \partial_t \eta = G, \tag{A3}$$

$$\nabla^2 v_z = \eta, \tag{A4}$$

$$\nabla^2 \phi = \nabla \cdot (\boldsymbol{v} \times \boldsymbol{e}), \tag{A5}$$

$$\partial_z^2 U - Re\, N (\boldsymbol{e} \cdot \boldsymbol{e}_z)^2 U - Re\, \partial_t U = Re\, [\partial_z \langle v_x v_z \rangle + P_X + N (\boldsymbol{e} \cdot \boldsymbol{e}_z) \Phi_Y], \tag{A6}$$

$$\partial_z^2 V - Re\, N (\boldsymbol{e} \cdot \boldsymbol{e}_z)^2 V - Re\, \partial_t V = Re\, [\partial_z \langle v_y v_z \rangle + P_Y - N (\boldsymbol{e} \cdot \boldsymbol{e}_z) \Phi_X]. \tag{A7}$$

The angular brackets $\langle\rangle$ denote horizontal averages. The mean-flow equations also contain the mean gradients of pressure and electric potential in x and y, namely P_X, P_Y and Φ_X, Φ_Y. The symbols F and G are given by

$$F = -Re\, \boldsymbol{e}_z \cdot [\nabla \times (\boldsymbol{v} \times \boldsymbol{\omega}) + N (\boldsymbol{e} \cdot \nabla)(-\nabla \phi + \boldsymbol{v} \times \boldsymbol{e})], \tag{A8}$$

$$G = Re[\partial_z \nabla \cdot (\boldsymbol{v} \times \boldsymbol{\omega}) - \boldsymbol{e}_z \cdot \nabla^2 (\boldsymbol{v} \times \boldsymbol{\omega}) + N (\boldsymbol{e} \cdot \nabla)^2 v_z], \tag{A9}$$

i.e. they originate from the nonlinear and Lorentz force terms. The boundary conditions at the channel walls are readily derived using $\nabla \cdot \boldsymbol{v} = 0$. We have

$$v_z = \omega_z = \partial_z \phi = \partial_z v_z = U = V = 0, \tag{A10}$$

where $\partial_z\, v_z = 0$ represents the boundary condition for the η-equation (A3).

For the time discretization of the evolution equations we use a method of second-order accuracy. If we write each equation symbolically as

$$\partial_t f = \mathscr{L} f + \mathscr{N}(f), \tag{A11}$$

where $\mathscr{L}$ denotes a linear operator and $\mathscr{N}$ the remaining terms, our time-stepping scheme

$$\frac{3f^{n+1}-4f^n+f^{n-1}}{2\Delta t}=\mathscr{L}f^{n+1}+2\mathscr{N}(f^n)-\mathscr{N}(f^{n-1}), \tag{A12}$$

where Δt is the time step. The left hand side approximates $\partial_t f$ at the time level $n+1$ using the previous two time levels. The linear term $\mathscr{L}f$ is treated implicitly, and $\mathscr{N}$ explicitly through the second-order Adams–Bashforth method, where the prefactors correspond to a linear extrapolation to the time level $n+1$. The first step from $n=0$ to $n=1$ is calculated with the Euler method.

The derivation of the discrete representation of (A2)–(A5) and for the mean-flow components (A6), (A7) proceeds in the same way as in Krasnov *et al.* (2004). We note that Φ_X, Φ_Y and P_Y have been set to zero. The driving pressure gradient P_X is adjusted at each time level such that the mass flux

$$Q_x=\int_{-1}^{1}U(z)\,\mathrm{d}z \tag{A13}$$

remains at a constant prescribed value. Details of the numerical algorithm and its parallelization are also discussed in Krasnov *et al.* (2004).

The flow solver has been verified for several test cases. First, we have reproduced the turbulent channel flow of Kim, Moin & Moser (1987) and Mansour, Kim & Moin (1988) with the Reynolds number based on the wall shear velocity $Re_\tau\approx 180$ (corresponding to $Re\approx 3300$ in the turbulent state) at a numerical resolution of 256 collocation points in all directions. Mean velocity profile, r.m.s. values of velocity perturbations, stress tensor components and dissipation rates of turbulent kinetic energy show perfect agreement with the results from Kim *et al.* (1987) and Mansour *et al.* (1988).

Secondly, we have conducted a cross-verification between linear and DNS solvers for Hartmann flow, i.e. with a wall-normal magnetic field. The results for transient growth of linear optimal perturbations by Gerard-Varet (2002) were reproduced with both codes for $Ha=20$ with $Re/Ha=200$, 500 and 1000 at the optimal wavenumber $\beta=1.0$. To achieve a linear regime with the DNS solver, the initial amplitude of optimal perturbations was chosen such that $E(0)=10^{-9}$. Another cross-verification was carried out for $\boldsymbol{e}=(\sqrt{0.5},\ 0.5,\ 0.5)$. We measured the energy amplification $\hat{G}$ at times $T=3.3$ and 5.0 for $Re=5000$, $Ha=20$ and wavenumbers $(\alpha,\beta)=(1,2)$. The initial perturbation energy was $E(0)=10^{-9}$ as in the previous case. The linear and DNS solvers yielded values $\hat{G}=11.1$ vs. 11.09 at $T=3.3$ and $\hat{G}=4.87$ vs. 4.868 at $T=5.0$ correspondingly, demonstrating good agreement between the two methods.

REFERENCES

Airiau, C. & Castets, M. 2004 On the amplification of small disturbances in a channel flow with a normal magnetic field. *Phys. Fluids* **16**, 2991–3005.

von Ammon, W., Gelfgat, Y., Gorbunov, L., Muhlbauer, A., Muiznieks, A., Makarov, Y., Virbulis, J. & Muller, G. 2005 Application of magnetic fields in industrial growth of silicon single crystals. In *15th Riga and 6th PAMIR Conf. on Fundamental and Applied MHD Modeling of MHD turbulence*, vol. I, pp. 41–54. Riga, Latvia.

Andersson, P., Berggren, M. & Henningson, D. S. 1999 Optimal disturbances and bypass transition in boundary layers. *Phys. Fluids* **11**, 134–150.

Barleon, L., Burr, U., Mack, K. J. & Stieglitz, R. 2001 Magnetohydrodynamic heat transfer research related to the design of fusion blankets. *Fusion Technol* **39**, 127–156.

Butler, K. M. & Farrell, B. F. 1992 Three-dimensional optimal perturbations in viscous shear flow. *Phys. Fluids* **4**, 1637–1650.

Canuto, C., Hussaini, M. Y., Quateroni, A. & Zang, T. A. 1988 *Spectral Methods in Fluid Dynamics*. Springer

Davidson, P. A. 1999 Magnetohydrodynamics in materials processing. *Annu. Rev. Fluid Mech.* **31**, 273–300.

Davidson, P. A. 2001 *An Introduction to Magnetohydrodynamics*. Cambridge University Press.

Farrell, B. F. & Ioannou, P. J. 1996 Generalized stability theory part I: autonomous operators. *J. Atmos. Sci.* **53**, 2025–2040.

Gerard-Varet, D. 2002 Amplification of small perturbations in a Hartmann layer. *Phys. Fluids* **14**, 1458–1467.

Gottlieb, D. & Orszag, S. A. 1977 *Numerical Analysis of Spectral Methods*. Philadelphia: SIAM.

Jimenez, J. 1990 Transition to turbulence in two-dimensional Poiseuille flow. *J. Fluid Mech.* **218**, 265–297.

Kim, J., Moin, P. & Moser, R. 1987 Turbulence statistics in fully developed channel flow at low Reynolds number. *J. Fluid Mech.* **177**, 133–166.

Krasnov, D. S., Zienicke, E., Zikanov, O., Boeck, T. & Thess, A. 2004 Numerical study of the instability of the Hartmann layer. *J. Fluid Mech.* **504**, 183–211.

Lee, D. & Choi, H. 2001 Magnetohydrodynamic turbulent flow in a channel at low magnetic Reynolds number. *J. Fluid Mech.* **429**, 367–394.

Luchini, P. 2000 Reynolds-number-independent instability of the boundary layer over a flat surface: optimal perturbations. *J. Fluid Mech.* **404**, 289–309.

Mansour, N. N., Kim, J. & Moin, P. 1988 Reynolds-stress and dissipation-rate budgets in a turbulent channel flow. *J. Fluid Mech.* **194**, 15–44.

Moreau, R. 1990 *Magnetohydrodynamics*. Kluwer.

Reddy, S. C., Schmid, P. J., Bagget, P. & Henningson, D. S. 1998 On the stability of stream-wise streaks and transition thresholds in plane channel flow. *J. Fluid Mech.* **365**, 269–303.

Roberts, P. H. 1967 *An Introduction to Magnetohydrodynamics*. Longmans, Green.

Schmid, P. J. & Henningson, D. S. 2001 *Stability and Transition in Shear Flows*. Springer Verlag.

Schmid, P. J. & Rossi, M. 2004 Three-dimensional stability of a Burgers vortex. *J. Fluid Mech.* **500**, 103–112.

Thomas, B. G. & Zhang, L. 2001 Mathematical modeling of fluid flow in continuous casting: a review. *ISIJ Intl* **41**, 1181–1193.

Zikanov, O. 1996 On the instability of pipe Poiseuille flow. *Phys. Fluids* **8**, 2923–2932.